ANALYTICAL MODELING OF A VACUUM FIELD EFFECT TRANSISTOR (VFET).

Thesis submitted as a partial requirement

for the completion of

Master of Science in Electrical and Electronic Engineering

By

Mehedy Hasan

Department of Electrical and Electronic Engineering

Bangladesh University of Engineering and Technology

Dhaka -1000, Bangladesh

(August, 2015)

CERTIFICATION

The thesis titled **–ANALYTICAL MODELING OF A VACUUM FIELD EFFECT TRANSISTOR (VFET).**" submitted by Mehedy Hasan, Roll No.: 0413062258 P, Session: April,2013 has been accepted as satisfactory in partial fulfillment of the requirements for the degree of **Master of Science in Electrical and Electronic Engineering** on August 10, 2015.

BOARD OF EXAMINERS

1. ……
Dr. Md. Ziaur Rahman Khan
Professor,
Department of EEE,
BUET, Dhaka
(Supervisor)
Chairman

2. ……
Dr. Taifur Ahmed Chowdhury
Professor & Head,
Department of EEE, BUET.
Member (Ex-Officio)

3. . ……
Dr. Quazi Deen Mohd Khosru
Professor,
Department of EEE,
BUET, Dhaka
Member

4. . ……
Dr. Muhibul Haque Bhuyan
Professor & Chairman,
Department of EEE,
Green University of Bangladesh,
Dhaka-1207
Member (External)

DECLARATION

It is hereby declared that this thesis or any part of it has not been submitted elsewhere for the award of any degree or diploma.

Signature of the candidate

_____

(Mehedy Hasan)

DEDICATION

To My Parents and Siblings

There are two possible outcomes. If the result confirms the hypothesis, then you have made a measurement. If the result is contrary to the hypothesis, then you have made a discovery.

- *Enrico Fermi (Italian Physicist and Discoverer of Fermi Level)*

Table of Contents

List of Figures

List of Tables

Constants

Electron Charge, q = $1.6\times10^{-19}\,coulomb$

Intrinsic Carrier Concentration in Silicon, n_i= $1.5\times10^{10}\,cm^{-3}$

Dielectric Constant of Silicon, $\in_{si} = 11.7\,\in_0$

Dielectric Constant of SiO_2, $\in_{ox} = 3.9\,\in_0$

Dielectric Constant of Free Space, $\in_0 = 8.854\times10^{-12}\,Fm^{-1}$

Plank's Constant, h= $6.63\times10^{-34}\,Js$

ACKNOWLEDGEMENTS

First of all, I am grateful to Almighty Allah for giving strength and courage to complete M.Sc thesis work.

I am highly pleased to express my sincere and profound gratitude to my M.Sc thesis Supervisor Dr. Md. Ziaur Rahman Khan, Professor, Department of Electrical and Electronic Engineering, Bangladesh University of Engineering and Technology (BUET) for providing me the opportunity to conduct my Masters research on Vacuum Field Effect Transistor (VFET). His helpful suggestion, continuous support and supervision inspired me throughout the process of the work.

I am grateful to my parents, friends and well wishers for their co-operation and support throughout the entire cycle of the work.

ABSTRACT

An analytical model has been developed for vacuum field effect transistor (VFET). Mathematical expressions for threshold voltage, drive in voltage and channel current have been derived. Threshold voltage of VFET has been obtained based on the minimum accumulation charges and minimum electric field. A drive in voltage has been modeled based on minimum current density for space charge limited emission. Analytical model of the channel current incorporates the device operating physics such as space charge limited emission and Fowler-Nordheim tunneling. Effective electric field and emission area have been determined to obtain channel current more accurately. The analytical model has been numerically verified with the practical simulated data available. Proposed model provides the opportunity to evaluate the vacuum device characteristics and determine the future projections as well. It can be a useful tool for analyzing different features of vacuum microelectronic devices.

Chapter 1

Introduction

1.1 Background

Back in the day (pre-1950s), vacuum tubes were commonplace in radios, televisions, computers, and other electronics. Today, you will have to look hard to find them. Their main function is to regulate the flow of electrons in electronic circuits and they look sort of like light bulbs as they are made of sealed glass and contain a heated filament. Unlike a light bulb, there are also a couple of electrodes above the filament — a metal grid and positively charged plate. The electrodes are separated by a vacuum, hence the name *vacuum tube*. Electrons flow from the heated filament, through the grid to the plate. This is referred to as *thermionic emission*. The grid can be used to interfere with the electron flow. Applying a small electric signal to the grid would lead to an amplified output signal thanks to the increased flow of electrons from the filament to the plate.

Peer inside an antique radio and you'll find what look like small light bulbs. They're actually vacuum tubes—the predecessors of the silicon transistor. Vacuum tubes went the way of the dinosaurs in the 1960s, but researchers have now brought them back to life, creating a nano-sized version that's faster and hardier than the transistor. It's even able to survive the harsh radiation of outer space.

Developed early last century, vacuum tubes offered the first easy way to amplify electric signals. Like light bulbs, they are glass bulbs containing a heated filament. But above the filament are two additional electrodes: a metal grid and, at the top of the bulb, a positively charged plate. The heated filament emits a steady flow of electrons, which are attracted to the plate's positive charge. The rate of electron flow can be controlled by the charge on the intervening grid, which means a small electric signal applied to the grid—say, the tiny output of a gramophone—is reproduced in the much stronger electron flow from filament to plate. As a resu , the signal is amplified and can be sent to a loudspeaker.

In the 1950s, transistors began to take the place of these vacuum tubes thanks to their small size and low power requirements. Transistor research evolved and eventually silicon transistors gained traction due to their low-leakage switching capabilities. Researchers have since been working to make these transistors smaller and smaller to meet the demand for faster, smaller, and less power-intensive electronics.

Vacuum tubes suffered a slow death during the 1950s and '60s thanks to the invention of the transistor—specifically, the ability to mass-produce transistors by chemically engraving, or etching, pieces of silicon. Transistors were smaller, cheaper, and longer lasting. They could also be packed into microchips to switch on and off according to different, complex inputs, paving the way for smaller, more powerful computers.

But transistors weren't better in all respects. Electrons move more slowly in a solid than in a vacuum, which means transistors are generally slower than vacuum tubes; as a result, computing isn't as quick as it could be. What's more, semiconductors are susceptible to strong radiation, which can disrupt the atomic structure of the silicon such that the charges no longer move properly. That's a big problem for the military and NASA, which need their technology to work in radiation-harsh environments such as outer space.

"The computer you and I buy is what NASA buys, but they won't want it exactly the same way," says Meyya Meyyappan, an engineer at NASA Ames Research Center at Moffett Field in California. "It takes them a few years to radiation-proof it. Otherwise the computer you put in the space shuttle or the space station basically will get zapped and stop working."

The new device is a cross between today's transistors and the vacuum tubes of yesteryear. It's small and easily manufactured, but also fast and radiation-proof. Meyyappan, who co-developed the "nano vacuum tube," says it is created by etching a tiny cavity in phosphorous-doped silicon. The cavity is bordered by three electrodes: a source, a gate, and a drain. The source and drain are separated by just 150 nanometers, while the gate sits on top. Electrons are emitted from the source thanks to a voltage applied across it and the drain, while the gate controls the electron flow across the cavity. In their paper published online today in *Applied Physics Letters*,

Meyyappan and colleagues estimate that their nano vacuum tube operates at frequencies up to 0.46 terahertz—some 10 times faster than the best silicon transistors.

The team's device isn't the first attempt at miniaturizing the vacuum tube. Contrary to previous work, however, the researchers do not need to create a "proper" vacuum: The separation of the source and drain is so small that the electrons stand very little chance of colliding with atoms in the air. This is a huge benefit, says Meyyappan, because it opens the door to mass production.

Electronics engineer Kristel Fobelets at Imperial College London agrees. "Vacuum technology within a semiconductor fabrication line would make fabrication costs very high," she says. Still, she cautions, the nano vacuum tube is more of a "proof of concept" than a working device, since its operational requirements do not yet match modern transistors. As one example, about 10 volts is needed to switch the device on, whereas modern transistors operate at about 1 volt; in this respect, the nano vacuum tube isn't compatible with modern circuits.

Even so, the potential is great, says Meyyappan. The new vacuum tube's inherent immunity to radiation could save the military and NASA a lot of time and money, while its faster operation makes it a rare candidate for so-called terahertz technology. Sitting between the microwave and infrared regions of the electromagnetic spectrum, the terahertz region can pick out the "fingerprints" of certain molecules. The technology could therefore be used at airports to safely scan for illicit drugs, for instance.

So are vacuum tubes poised to make a comeback? Meyyappan thinks so. "We are combining the best of the vacuum," he says, "and the best of what we have learned in the past 50 years about integrated-circuit manufacture."

The vacuum transistor looks very similar to a MOSFET, with a source, drain, gate, and insulator. In the case of a MOSFET, a voltage is applied to the gate, which generates an electric field in the semiconductor material (silicon, typically) below the gate. Current then flows in the channel between the source and drain, but never into the gate, thanks to the insulating oxide layer.

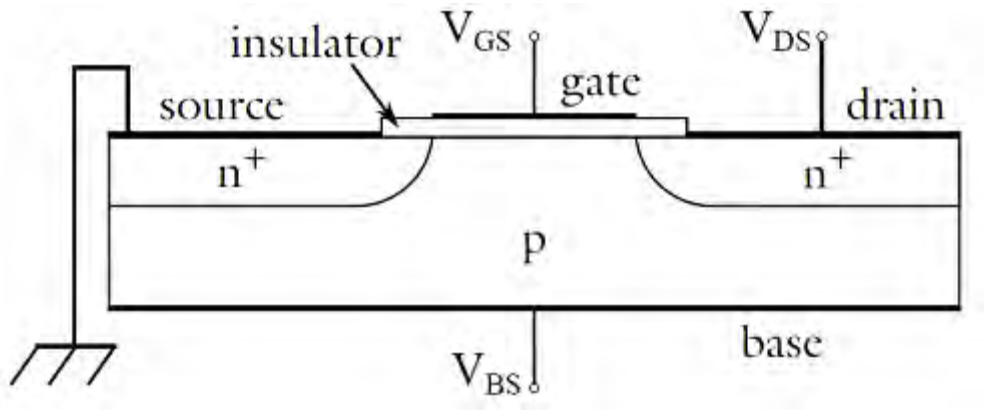

Figure 2.1 : Concept of a MOSFET.

The main difference between a MOSFET and the new vacuum transistor is that the electrons flow from the source to the drain through a vacuum instead of silicon. Unlike the vacuum tube, the distance between the source and the drain is small enough in the vacuum transistor that you do not need to heat the gate. Instead, electrons flow by way of *field emission*.

This is a big deal, as the race to make smaller and more powerful transistors has long been restricted by the need for silicon. Until the vacuum transistor, instead of eliminating the semiconductor material, what kept shrinking was the insulating oxide layer. Because of the MOSFET‘s design, the insulator cannot keep shrinking until it‘s gone. The vacuum transistor would supposedly solve this issue.

NASA has filed a patent on a unique gate insulated vacuum channel transistor. The vacuum transistor is created using standard silicon semiconductor processing. This is done by etching a tiny cavity in phosphorous doped silicon, bordered by three electrodes; a source, a gate, and a drain. The channel length is 150nm, with the gate on top. Electrons are emitted from the source due to a voltage applied across it and the drain, while the gate controls the electron flow across the cavity. When the gap between the source and drain is of the order of 150nm the electrons do not collide. The mean free path of the electrons (the average length an electron can travel before hitting something) is more than 1μm.

Advantages of the vacuum tube and transistor are combined here through nanofabrication. A photoresist ashing technique enables a nano-gap separation of the emitter and the collector, thus allowing operation at less than 10V. This allows high frequency and power output while

satisfying the metrics of lightness, cost, lifetime, and stability at harsh conditions. The operation voltage can be decreased comparable to modern semiconductor devices. This patented technology is available for licensing from NASA‘s space program to benefit U.S. industry.

1.2 Literature Review

High-speed electronic devices rely on short carrier transport times, which are usually achieved by decreasing channel length and increasing carrier velocity [1-2]. It is difficult to achieve ballistic transport in a solid-state medium because high electric fields used to increase carrier velocity also increase scattering [3-4]. The vacuum is intrinsically superior to solid as carrier transport medium since it allows ballistic transport. Early electronics centered around the vacuum tube used to amplify, switch or modulate electrical signals [5-6]. The transition from vacuum tube to solid-state device was driven by the ease of fabrication, low cost, low-power consumption, lightness, long lifetime, and ideal form factor for integrated circuits [7].

The advantages of both devices can be achieved together if macro-scale vacuum tube is miniaturized to nanometer scale [8]. The nano vacuum tubes can provide high frequency/power output and provide stability at harsh conditions [9-10]. Further downscaling can allow a cold cathode because the electric field itself is strong enough to emit electrons [6]. Also, downscaling in conjunction with low work function materials may decrease the turn-on gate and drain voltages, thus enabling devices to be competitive with modern semiconductor technology [8].

1.3 Objective of This Thesis

The objectives of this thesis are:

- To obtain an analytical model for turn on / threshold gate voltage and drive in voltage in anode / collector.
- To analyze the voltage current characteristics due to space charge limited emission and quantum tunneling.
- To obtain an analytical model for ON current density in VFET.
- To investigate the effect of field enhancement factor in cathode with sharp tip.

1.4 Thesis Methodology

The electron flow through a metal nano-gap structure usually involves a two-step process: field emission from the metal surface, commonly described by Fowler–Nordheim theory and subsequent transport through the gap, governed by Child–Langmuir SCL current flow. The Child–Langmuir law assumes zero normal field at the cathode surface, whereas Fowler-Nordheim emission requires a surface-normal field of significant strength. In a variety of electron devices, the charge densities are sufficiently large that the self-consistent effects of the charges on themselves as well as the applied fields must be considered. Solution to classical space-charge-limited emission will be done by solving second-order nonlinear Poisson‘s equation. Field emission due to tunneling will be determined from Fowler-Nordheim equation. We need to incorporate the field enhancement criteria as electric field is strongest along the surface where object is most curved. To do so, field enhancement factor will be used to determine the effective field at cathode tip.

Like well-defined FET characteristics nano-void channel must have a turn on threshold voltage. Below threshold, the channel current remains off even at with a high anode voltage. This is the minimum voltage required at gate to accumulate enough charge for field emission. The threshold voltage will be modeled using basic electromagnetics. Above threshold, the channel current turns on and reveals a $V^{3/2}$ dependence on the anode to cathode voltage. Electrons emitted from the inversion layer in cathode are accelerated by the electric field developed between the anode and cathode edges and travel ballistic in the nano-void channel region. Minimum voltage required for this transport is called drive in voltage, which will be modeled using the physics of space charge limited emission. For same bias voltage in anode and gate, the channel current remains flat, with a level solely determined by gate voltage. All simulations will be done in MATLAB.

1.5 Thesis Map

The dissertation consists 5 chapters. Chapter 1 includes introduction of vacuum devices, vacuum device benefits and challenges, emerging vacuum technology roadmap. It also discusses the objective of this thesis and highlights on related previous works.

Chapter two discusses the background of vacuum microelectronics, VFET device introduction, device structure and modes of operation. Also it includes device operating physics of space charge limited emission and mechanisms of quantum tunneling.

Chapter three contains analytical model of VFET. It includes mathematical expression for threshold and driving voltage along with the on current equation of the device. It also depicts the process of obtaining effective electric field and emission area of cathode.

Chapter four includes the results and discussion of the analytical model. The proposed analytical model for threshold voltage and channel current is numerically verified here by the simulation data available.

The last chapter concludes the thesis with a summary of the work. It also brings up the related current work and scopes for future work related to vacuum device technology.

Chapter 2

Vacuum Microelectronics

2.1 Background

When semiconductor transistors were invented by Bardeen, Brattain, and Shockley in the 1950s [11], and integrated circuits were subsequently developed in the 1960s [12,13], people generally thought that the time of using vacuum tubes was over. They were large, fragile, and inefficient. They required a vacuum to operate and used a cathode heated to over 1000°C to generate the electrons. However, the emergence of vacuum microelectronic (VME) devices has generated renewed interests in the exploitation of vacuum tubes for many new applications. Vacuum microelectronics, a new interdisciplinary science and technology, deals with vacuum devices of micrometer dimensions that are made by microfabrication techniques developed for the semiconductor industry. To help understand the evolution of this technology, let‘s discuss some historical developments that occurred in this field.

2.1.1 Shoulders' Proposal

Historically, there were two important technological breakthroughs that made the birth of modern vacuum microelectronics possible. The first was the microfabrication technology developed for on-chip large scale integration of micron-sized solid-state devices. If a vacuum triode that was manually machined and assembled 40 years ago could be operated at frequencies as high as 4 GHz [14], it would not be difficult to imagine that the new microfabrication techniques, which could produce devices with dimensions three orders of magnitude smaller, would enable much faster speeds for VME devices.

About 40 years ago, Shoulders of Stanford Research Institute (SRI) presented a device concept in an article entitled ―Microelectronics using electron-beam-activated machining techniques" [15]. At that time, the microfabrication technology that we know today had not come to existence, and Fairchild Corporation had just announced its 4-transistor monolithic chips with a newly invented planar process [16]. However, Shoulders, with tremendous vision and insight,

proposed ~~to~~ devise vacuum tunnel effect devices of micron sizes with switching times in 10^{-10} s that

(i) Operate at 50 V

(ii) Have high input impedance,

(iii) Are insensitive to temperature effects up to 1000°C,

(iv) Are insensitive to ionizing radiation effects up to the limits of the best known dielectric materials

(v) Have a useful lifetime of many hundreds of years."

The proposed device structure was exactly what the microfabrication technology was developed to create. The powerful combination of the field emission cold cathode with the microfabrication techniques would seem to be capable of overcoming most of the drawbacks associated with the traditional vacuum tubes. It is an irony, though, that while semiconductor electronics advanced rapidly soon after the time of Shoulders' publication, vacuum microelectronics took 40 years to get off the ground. Nevertheless, his power of technological imagination was truly gigantic.

2.1.2 Groundbreaking Work

Field emission was traditionally studied within the discipline of surface science. The early history of surface science was full of studies of cathodes, which led to many important discoveries. For example, Langmuir's adsorption isotherm for gas–solid surface interactions [17], which essentially laid the foundation of modern surface science, was a direct result of his studies on heated tungsten filaments. The experiment conducted by Davisson and Germer in 1927 [18], which established the wave nature of electrons, was originally designed to investigate the role of positive ion bombardment in electron emission from oxide-coated nickel cathodes used in vacuum triode amplifiers. Later, this work also led to the discovery of low energy electron diffraction (LEED) [19].

Armed with the ~~n~~ew" quantum mechanics, Fowler and Nordheim calculated a relationship between the emission current density and the applied electric field in 1928 based on electron tunneling through a simple two-dimensional (2-D) triangular barrier [20-21]. However, experimental verifications of the theory were not easy because of the need for very high electric fields. It was also difficult at the time to obtain field emission under controlled and reproducible conditions, due to the perturbing effects of invisible micro-structural defects and impurities on

the emitter surfaces. Catastrophic vacuum arcs often occurred between electrodes at high voltages. In fact, how high a voltage could be applied between electrodes without causing a vacuum arc had become a critical design issue at that time for all types of vacuum devices ranging from cathode ray tubes to high-energy accelerators. These vacuum-breakdown phenomena and associated physical mechanisms were topics of intensive research in the 1950s–1960s [22].

As indicated earlier, it was necessary to employ a sharp needle for obtaining a sufficiently high electric field for electron emission. In 1937, Muller etched a fine tungsten wire and placed it at the center of a spherical glass vessel, the inside surface of which was coated with a fluorescent material [23]. He observed a symmetric pattern on the fluorescent screen produced by field emitted electrons that traveled radically from the tip to the screen. This was essentially the field emission microscope (FEM) that we know today. Using this FEM setup, Good and Muller and Dyke and Dolan [24] examined and verified the Fowler–Nordheim equation over a wide range of currents and voltages. Because of the strong dependency of current density on the local electric field and the work function of the emitter surface, both of which were sensitive to the atomic structure and any adsorbates at the surface, this field emission apparatus also became an excellent tool for studying surface phenomena such as crystallographic structure, chemisorption, surface diffusion, and impurity effects. Etched needles have been successfully deployed in many devices such as microwave amplifiers, high-resolution cathode ray tubes, electron microscopes, electron beam lithography, and flash X-ray photography [25].

2.1.3 Invention of Spindt Cathode

By the mid-1960s, excitement and enthusiasm for Shoulders‘ concept of microminiaturized vacuum tubes incorporating a field emission electron source had waned considerably, mainly because technical difficulties encountered in using etched needles as electron emitters in such devices had stalled any momentum. Then, Spindt of SRI, who was hired by Shoulders to carry on the work, displayed unyielding persistence in pursuing the device concept and finally succeeded in fabricating the field emitters that Shoulders had dreamed of. The first publication of his work appeared in 1968, and the emitters, now known as the Spindt cathode, consisted of a multilayer structure of Mo gate/SiO2 insulator/Mo cathode cones on a Si substrate fabricated by thin film vacuum deposition techniques. The technology allowed the emitters to be fabricated in

arrays of up to many thousands tips at a packing density of tens of millions per square centimeter. An extensive review of the general properties of Spindt cathodes, also commonly referred to as field-emitter arrays (FEAs), was published in 1976.

There were variations to the cone-shaped Spindt metal emitters, both geometrically, such as wedge and thin film edge emitters, and materials-wise, such as carbides and semiconductors. In particular, Gray of Naval Research Laboratory fabricated a structure called ―vacuum field effect transistor" based on Si-FEAs in 1986. The structure consisted of emitters, gates, and collectors on the same planar surface of a silicon wafer and exhibited both voltage and power gains with a transit time of only 5 ps from the emitter to the collector. This was a fine example of the use of state-of the- art silicon fabrication technology in building advanced vacuum microelectronic devices. In addition to the great variety of available fabrication techniques, the I –V characteristics of semiconductor-FEAs could be made different from those of metal-FEAs. This opened up new application fronts, including light-sensitive FEAs, electron velocity-saturated FEAs, noble metal-silicided tip-FEAs, and monolithically integrated FEAs with silicon and optoelectronic integrated circuits [26].

2.2 Field Emitter Arrays

The first 6 years following the 1st International Vacuum Microelectronics Conference (IVMC, from 1988 to 1993) could be called the ―Years of the Spindt Cathode," because attention was almost entirely devoted to the characterization and understanding of Spindt-type FEAs and their practical applications. Researchers probed all types of issues in an effort to optimize the technology so that one can ―draw the most current at the least applied voltage from the smallest device structure". There were many notable breakthroughs reported in this period that had far-reaching implications for the technology. For example, Van Veen of Philips Research Labs reported the largest current obtained from a single Mo tip: 850 μA at a gate voltage of 205 V [27]. Spindt reported the highest current of 6mAdrawn from a 12 tip Mo-FEA, which was equivalent to a current density of 320 A/cm^2 or 500 μA/tip. He further found that when the number of tips increased, the average emission current per tip actually decreased due to variations in tip geometry. A 5000-tip FEA yielded a total current of 100 mA, which corresponded to ~ 20μA/tip.

Bozler et al. of MIT Lincoln Laboratory fabricated the smallest-dimension Mo-FEAs at the time using inter-ferometric lithography, featuring a gate-to-tip distance of 0.08μm, a tip-to-tip distance of 0.32 μm, and a tip density of 109/cm^2. They measured a current of 1μA (1nA/tip or 1 A/cm^2) at 25 V from an uncesiated 10 × 10μm array of 900 tips, a record low gate voltage for FEAs. The cesiated array achieved 1μA at an even lower voltage of 10 V, and the maximum current density reached 1600 A/cm2, again a record for FEAs. Schowebel et al. [28] reported that treating the emitters in hydrogen plasma was effective in removing surface contaminants and enhancing the emission uniformity. This emitter pre-conditioning has become a standard procedure in the processing of FEAs. Gomer, Spindt et al., and Goodhue et al. [29] did extensive work in understanding the nature of emission noise from FEAs. They identified that emission predominantly originated from nano-scale protrusions on the tip surface, and the change of atomic structures at these protrusions because of enhanced surface diffusion in high electric fields led to discrete jumps in emission current, and hence the occurrence of flip-flop or flicker noises.

2.3 New Cathode Materials

In the subsequent IVMC years (1994–2000), there has been a noticeable shift in research activities. Besides the strong push in FEA-based FEDs by companies such as Pix-Tech and Candescent Technologies, researchers have been increasingly turning their attentions to the search for new cathode materials. The main motivation is to find materials or structures that are more robust and manufacturing-friendly than the FEAs. Of the many reported cathode materials, diamond and carbon nanotube emitters have attracted the most interest. As an example, nearly one-third of the conference papers were on diamond related work at the 10th IVMC (Kyongju, Korea) in 1997.

Diamond, with its negative electron affinity (NEA) on hydrogen-terminated surfaces and the ability of depositing it in thin film forms at low pressures by chemical vapor deposition, has been shown to exhibit low emission threshold fields of 3–40 V/μm for a current density of 10mA/cm2. These values compare favorably to those required for metal or semiconductor FEAs. Similarly, the one-dimensional carbon nanotubes, which are nanometers in diameter (1–30 nm) and micrometers in length (1–20μm), are also low-field emitters. Emission currents as high as 1μA from single nanotubes [30] and current densities as high as 4 A/cm^2 from multiple nanotubes

[31] have been observed. It is interesting to note that the emitting structure of nanotubes has been speculated to consist of a single atomic chain of 10 to 100 carbon atoms that are pulled out from an open graphene sheet at the nanotube end by the strong local electric field. This may prove to be the ultimate atomic-scale field emitter structure that researchers have been searching for. Active development efforts on diamond and carbon nanotube-based FEDs and lighting elements are ongoing at a number of companies, including SI Diamond Technology, Samsung, and ISE Electronics [32].

2.4 Vacuum Field Effect Transistor (VFET)

Early electronics centered around the vacuum tube used to amplify, switch, or modulate electrical signals. It has been many decades since the vacuum tubes have been replaced by solid-state devices such as the metal-oxide-semiconductor field-effect transistor (MOSFET) and diode. Nevertheless, the vacuum tubes are still used in niche applications such as premier sound systems and high-power radio base stations [10]. The transition from the vacuum tube to the solid-state device was not driven by the superiority of the semiconductor as a carrier transport medium but by the ease of fabrication, low cost, low-power consumption, lightness, long lifetime, and ideal form factor for integrated circuits (ICs). The vacuum tubes were fabricated by mechanical machining and used as discrete components, whereas modern solid-state devices are batch processed in assembling the integrated circuits. The vacuum device is more robust than solid-state devices in extreme environments involving high temperature and exposure to various radiations. The critical tradeoff is that the vacuum tubes yield higher frequency/power output but consume more energy than the MOSFET. The vacuum is intrinsically superior to the solid as carrier transport medium since it allows ballistic transport while the carriers suffer from optical and acoustic phonon scattering in semiconductors. The velocity of electrons in vacuum is theoretically $3x10^{10}$ cm/s, but is limited to about $5x10^{7}$ cm/s in semiconductors. As the cathodes of vacuum tubes need to be heated for thermionic emission of electrons, the energy for heating adversely overwhelms the energy required for field emission. The vacuum device is, therefore, not suitable for low power devices. For high power amplification (>50 W), however, the solid state device needs a complex circuit architecture including many transistors, micro-strips, and thermal management systems.

The advantages of both devices can be achieved together if the macro-scale vacuum tube is miniaturized to the nanometer scale. The nano vacuum tubes can provide high frequency/ power output while satisfying the metrics of lightness, cost, lifetime, and stability at harsh conditions. More importantly, further downscaling can allow a cold cathode because the electric field itself is strong enough to emit electrons. Also, an ultimate downscaling in conjunction with low work function materials may decrease the turn-on gate and drain voltages to less than 1V, thus enabling these devices to be competitive with modern semiconductor technology. These benefits can be attained by the use of matured IC technology to fabricate nanoscale vacuum tubes and facilitate circuit integration.

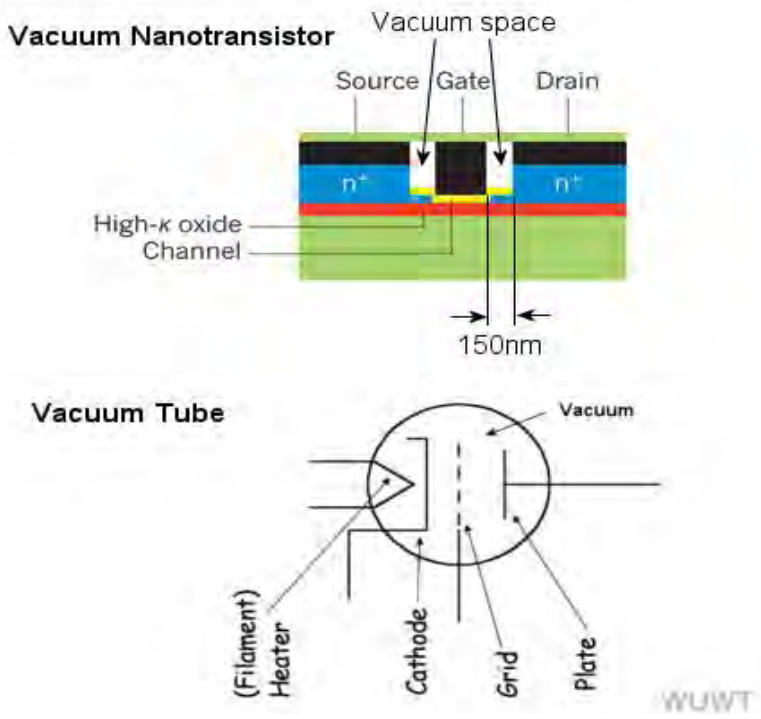

Figure 2.1 : Vacuum Nano-transistor & Vacuum Tube [5]

2.5 VFET Structures

The most common design of vacuum microelectronic is a vertical field emitter consisting of the emitter, gate, and collector as shown in Fig. 2.2(a). The emitter is a sharp conical tip, the gate is a circular aperture, and the collector is flapped at the top. The movement of electrons between the emitter (cathode) and the collector (anode) is controlled by the gate. An array of vertical field

emitters forms a large-area flat electron source [33]. Unfortunately, the vertical structure may be undesirable for circuit implementation due to the difficulties in achieving geometrical dimensions such as gap spacing to be identical over all devices on the substrate. In contrast, the geometry of the planar structure (Fig. 2.2(b)) is defined by photolithography enabling practical integration [34]. However, as the distance between the emitter and the gate shrinks, processing becomes difficult. In addition, a fraction of the emitted electrons can be easily swept into the gate, as well as the electrons at the gate can be emitted to the collector, both of which are detrimental in circuit design. Herein, we have implemented a gate-insulated planar lateral triode to reduce the gate leakage similar to silicon dioxide in MOSFET preventing the gate leakage current. Figures 2.2(c) and 2.2(d) show the structural analogy between the back-gate MOSFET and our nano vacuum channel transistor.

The device was fabricated via conventional semiconductor fabrication techniques. The space between the emitter and the collector was defined less than the lithography limit, achieved by photoresist ashing. As the channel distance becomes less than the mean free path of electrons in air, the vacuum requirement itself is relaxed, and the field emission voltage is reduced to a value smaller than the ionization potential of molecules in air. As such, the present device can be referred to as the vacuum channel transistor even though it operates at atmospheric conditions.

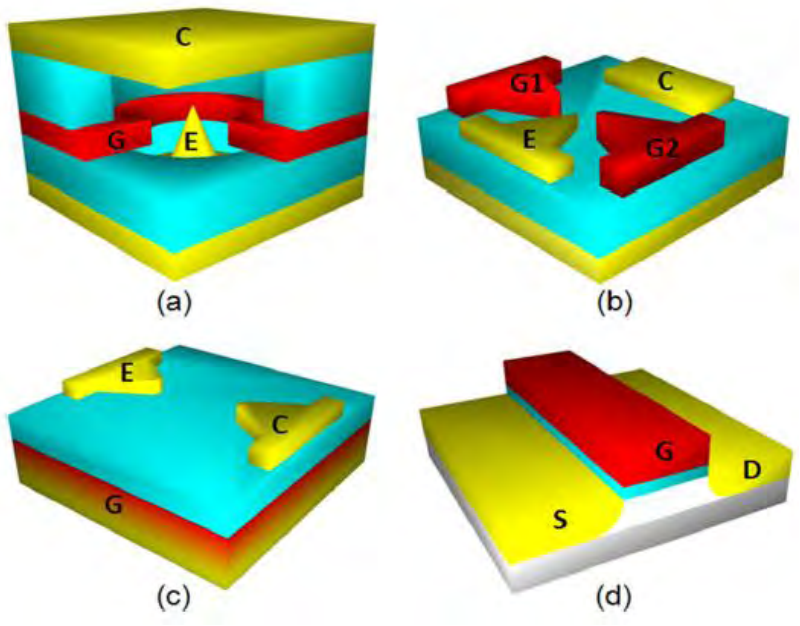

Figure 2.2 : Structures of Vacuum Devices.
(a) Vertical Field Emitter, (b) Plananr Lateral Field Emitter,
(c) MOSFET, (d) Gate insulated air channel transisitor.
Figure taken from [7].

2.6 Space Charge Limited Current

It has been known for nearly a century that there is an upper limit on the amount of current that can pass between two electrodes. This limiting current is known as the space-charge limited (SCL) current and is one of the most important phenomena related to charged particle beams. For beam currents below this limit, the beam flow is laminar through the drift space and the problem is time-independent. However, if the beam current exceeds the SCL current a virtual cathode is formed and the transmitted current decreases. The virtual cathode is a point where a fraction of the beam particles come to rest and represents instability in the beam. After the formation of a virtual cathode, the transmitted current decreases as the injected current increases. The ability to accurately determine the SCL current, in order to prevent or enhance the formation of a virtual cathode, is required in several fields, including high-power microwave devices[35], astrophysical plasmas, xerographic technology, electron beam ion sources and traps[36], field emitter arrays, and collective-ion acceleration. For most high-power microwave (HPM) devices the presence of a limiting current represents a limitation in the ability to produce microwave energy since an arbitrarily large electron beam current is not possible. On the other hand, the vircator (VIRtual Cathode oscillATOR) and reflex triode use the presence of the virtual cathode as a means for microwave production. In astrophysical plasmas, electric fields established in pulsar magnetospheres and white dwarf accretion disks are expected to establish currents that are space-charge limited. Similar to simple diodes, xerographic devices employ a potential difference to transport resin particles from a donor electrode to the receiver electrode as a means to transfer images. Electron beam ion sources/traps use the potential depression of an electron beam to trap and/or create high charge state ions. High density beams, i.e., large current densities, are required to obtain high ionization efficiencies. The SCL current is one limitation that must be considered.

Field emitter arrays ~~h~~old the potential for significantly impacting next-generation radio frequency amplifiers." Employing numerous conical emitters and applying a larger potential difference between the gate electrode and anode, large current densities are possible and understanding the effects of space-charge on the current flow is essential. Collective ion accelerators use a propagating virtual cathode formed within a high energy electron beam to accelerate the ions. Thus, it is clear that knowledge of the space-charge limited current and the

ability to predict it for a variety of beam and drift space geometries is important throughout physics.

2.6.1 History of SCL Current

The first published accounts of SCL currents is due to Child in 1911 and Langmuir [37-38], a few years later, who investigated the current flow between planar electrodes with a potential difference insufficient to saturate the region. The first exact treatment of the relativistic Child-Langmuir problem was given by Jory and Trivelpiece in 1969. They considered a one dimensional planar diode with a cold, mono-energetic beam of electrons injected from the cathode. Using elliptic integrals, they developed an analytic expression for the limiting current that reduces to the Child-Langmuir law in the non-relativistic regime. Recently, temperature effects were included in both a non-relativistic[28] and a relativistic extension to the Child-Langmuir law. Unfortunately, the resulting equations had to be numerically solved. Since most HPM devices use cylindrical or toroidal drift spaces, the need for formulas that considered more than one dimension increased. Unfortunately, self consistently solving Poisson‘s equation for SCL flow for anything other than a one dimensional planar problem requires a numerical approach. Bogdankevich and Rukhadze considered finite-length effects for electron beams in hollow drift tubes. Using a linearization of the two-fluid hydrodynamic equations, they investigated the stability of both uncompensated and compensated (filling the drift tube with positive ions to reduce the electron space-charge) beams. Later, Voronin *et al* [39] devised a method to estimate the SCL current, including length-effects.

2.6.2 Physics of Space-Charge Limited Current Flow

Following a qualitative description of the space-charge limit, illustrated in Figure 2.3. The first electrons in a beam leaving an emitter move freely across the emission gap to their target: i.e., across a vacuum gap to an anode or across a positively-biased sheath to the plasma surrounding a spacecraft. Subsequent electrons, however, are influenced by the negative electric field generated by each electron already in the beam, causing them to decelerate. This is referred to as a space-charge effect. The impact of each emitted electron is cumulative such that, as the emission current increases, so does the deceleration force. The deceleration of electrons creates volume of

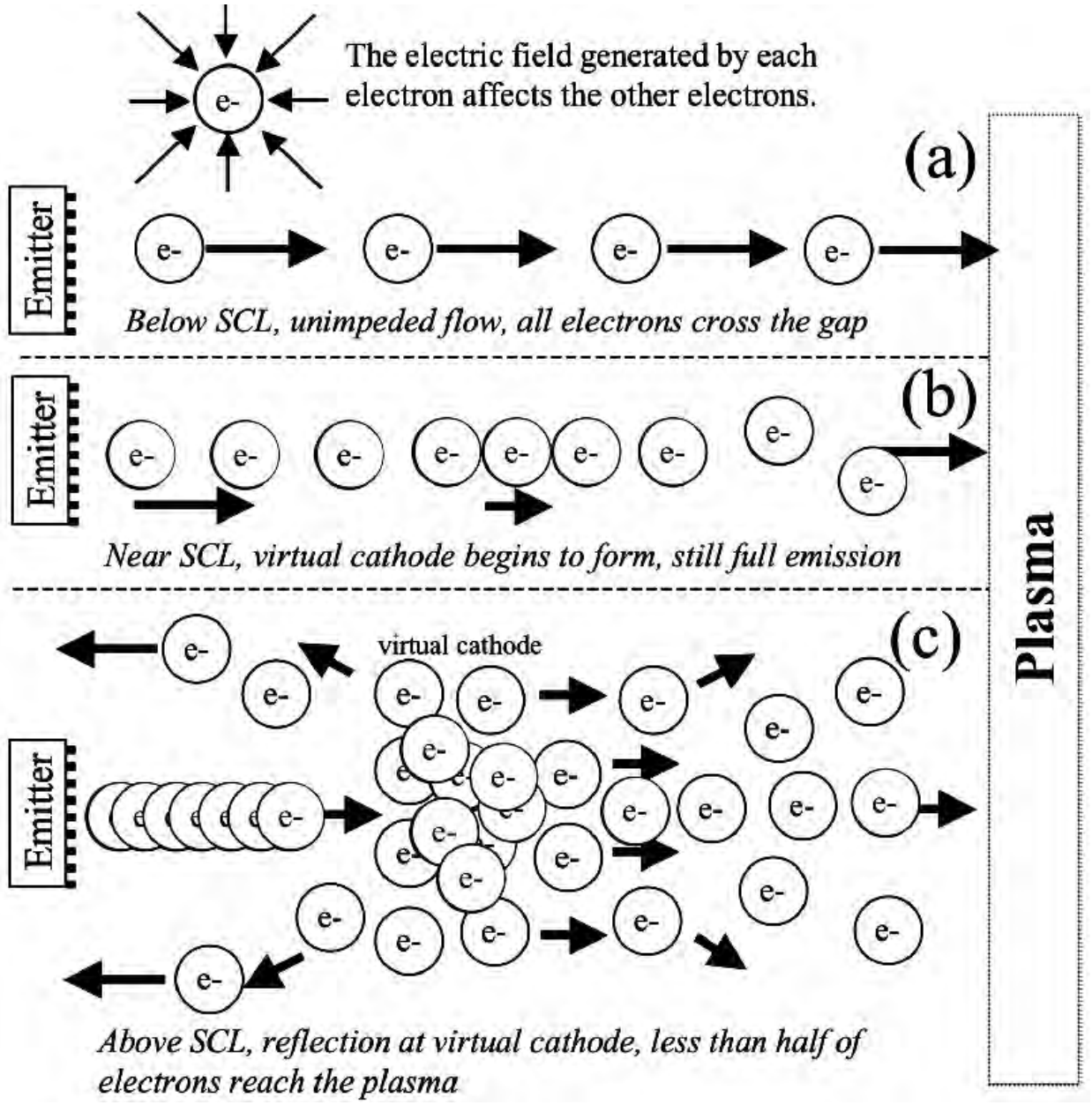

Figure 2.3 : Graphical depiction of the space-charge limit for electron emission from a space-craft cathode [11]

increased beam density in the emission gap where electrons reach their minimum velocity. At low currents, electrons decelerate as they approach this increased density and re-accelerate after they pass it. The distribution of electron velocities spreads, but the peak velocity at the far side remains as high as the peak velocity at the emitter. At sufficiently high currents, however, the velocity of the slowest electrons drops to zero and below. Once this occurs, the charge at the

high density point in the beam, referred to as the virtual cathode, builds up rapidly. Next, more and more subsequent electrons approaching the virtual cathode are reflected back to the emitter. Simultaneously the virtual cathode expands as its self-field pushes it apart in all directions. Thereafter, the virtual cathode forms and dissipates in a time varying pattern. The current above which this occurs is referred to as the space-charge limit.

This simple description of the space-charge limit ignores the voltage across the gap, as well as other effects, but it serves to illustrate the basic space-charge concept. Emission below the space-charge limit is efficient- even though electrons are decelerated at the forming virtual cathode, they do not stop or reflect (though they may spread laterally), and essentially all of the emitted electrons successfully cross the gap. When the space charge limit is reached, however, the potential at the virtual cathode is sufficient to stop and reflect most of the incoming electrons.

2.6.3 Derivation of Space Charge Current Density

Current density,

$$J(z) = \rho(z)v(z) = -J_{SCL} \quad \ldots\ldots\ldots\ldots\ldots\ldots\ldots\ldots\ldots\ldots\ldots\ldots\ldots\ldots (2.1)$$

For the motion of an electron, we can write,

$$\frac{1}{2}mv^2(z) - e\phi(z) = 0 \quad \ldots\ldots\ldots\ldots\ldots\ldots\ldots\ldots\ldots\ldots\ldots\ldots\ldots\ldots (2.2)$$

Poisson's equation,

$$\frac{d^2\phi}{dz^2} = -\frac{\rho(z)}{\epsilon_0}$$

$$= \frac{J_{SCL}}{\epsilon_0}\frac{1}{v(z)}$$

$$= \frac{J_{SCL}}{\epsilon_0}\sqrt{\frac{m}{2e}}\frac{1}{\left(\sqrt{\phi(z)}\right)} \quad \ldots\ldots\ldots\ldots\ldots\ldots\ldots\ldots\ldots\ldots (2.3)$$

Multiplying eqn. (3.3) $\left(\frac{d\phi}{dz}\right)$ on both sides,

$$\frac{d^2\phi}{dz^2}\frac{d\phi}{dz} = \frac{J_{SCL}}{\epsilon_0}\sqrt{\frac{m}{2e}}\frac{1}{\left(\sqrt{\phi(z)}\right)}\frac{d\phi}{dz} \quad \ldots\ldots\ldots\ldots\ldots\ldots\ldots\ldots\ldots\ldots\ldots\ldots (2.4)$$

Integrating eqn. (3.4),

$$\left(\frac{d\phi}{dz}\right)^2 = 2\,\frac{J_{SCL}}{\epsilon_0}\sqrt{\frac{m}{2e}}\int \frac{1}{\left(\sqrt{\phi(z)}\right)}\frac{d\phi}{dz} \quad \text{………………………………} (2.5)$$

Using boundary conditions,

$$\left(\frac{d\phi}{dz}\right)^2_{z=z} = 4\,\frac{J_{SCL}}{\epsilon_0}\sqrt{\frac{m}{2e}}\sqrt{\phi(z)} + \left(\frac{d\phi}{dz}\right)^2_{z=0}$$

$$\Rightarrow \left(\frac{d\phi}{dz}\right)^2 = 4\,\frac{J_{SCL}}{\epsilon_0}\sqrt{\frac{m}{2e}}\sqrt{\phi(z)}$$

$$\Rightarrow \left(\frac{d\phi}{dz}\right) = \sqrt{4\,\frac{J_{SCL}}{\epsilon_0}}\left(\frac{m}{2e}\right)^{\frac{1}{4}}[\phi(z)]^{\frac{1}{4}}$$

$$\Rightarrow \left(\frac{d\phi}{[\phi(z)]^{\frac{1}{4}}}\right) = \sqrt{4\,\frac{J_{SCL}}{\epsilon_0}}\left(\frac{m}{2e}\right)^{\frac{1}{4}} dz$$

Integrating again,‘8

$$\Rightarrow \left(\frac{4}{3}[\phi(z)]^{\frac{3}{4}}\right) = \sqrt{4\,\frac{J_{SCL}}{\epsilon_0}}\left(\frac{m}{2e}\right)^{\frac{1}{4}} z$$

$$\Rightarrow \phi(z) = \left(\frac{3}{2}\right)^{\frac{4}{3}}\left(\frac{J_{SCL}}{\epsilon_0}\right)^{\frac{2}{3}}\left(\frac{m}{2e}\right)^{\frac{1}{3}} z^{\frac{4}{3}}$$

$$\Rightarrow J_{SCL} = \frac{4}{9}\,\varepsilon\sqrt{\frac{2e}{m}}\,\frac{\phi(z)^{\frac{3}{2}}}{z^2} \quad \text{………………………………………….} (2.6)$$

Boundary condition,

For,	z = 0	$\phi(z) = 0$	→	Cathode
For,	z = D	$\phi(z) = V$	→	Anode

Final equation for current density,

$$J_{SCL} = \frac{4}{9}\,\varepsilon\sqrt{\frac{2e}{m}}\,\frac{V^{\frac{3}{2}}}{D^2} \quad \text{………………………………} (2.7)$$

2.6.4 Two and Three Dimensional Space-charge Limits

More detailed analysis indicates that significant improvement to the one-dimensional space-charge limit can be attained when the spreading of the emitted electrons in multiple dimensions is considered. Luginsland et al. [1996] shows that the improvement depends upon the width of the emitter relative to the emission gap as per the following equation. The situation modeled is shown in Figure 2.4.

$$\frac{J_{cl}(2)}{J_{cl}(1)} = 1 + \frac{0.3145}{\frac{W}{D}} - \frac{0.0004}{\left(\frac{W}{D}\right)^2} \quad \ldots\ldots\ldots\ldots\ldots\ldots\ldots\ldots\ldots\ldots\ldots\ldots\ldots\ldots (2.8)$$

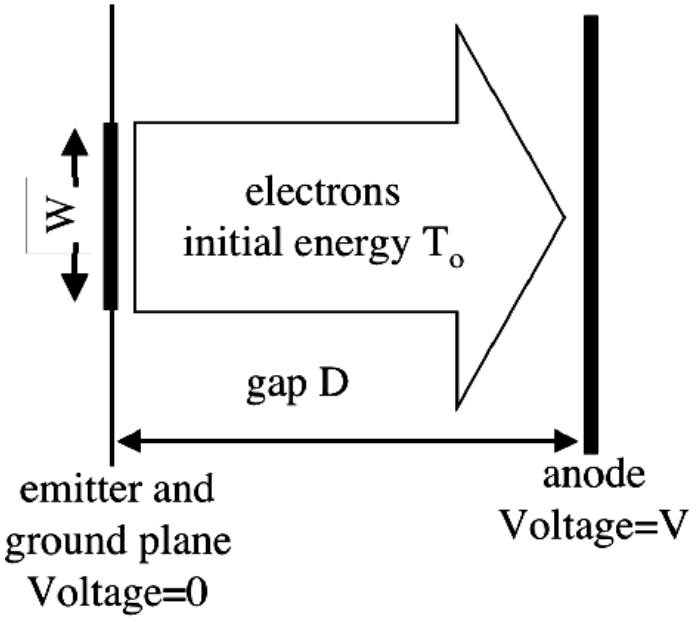

Figure 2.4 : Side-view of the two dimensional geometry for space-charge limit calculation [39]

To illustrate the progression from the two-dimensional to the three-dimensional models, Figure 2.5 shows the two-dimensional and three-dimensional situations in the context of a spacecraft emitter sending electrons into the surrounding plasma.

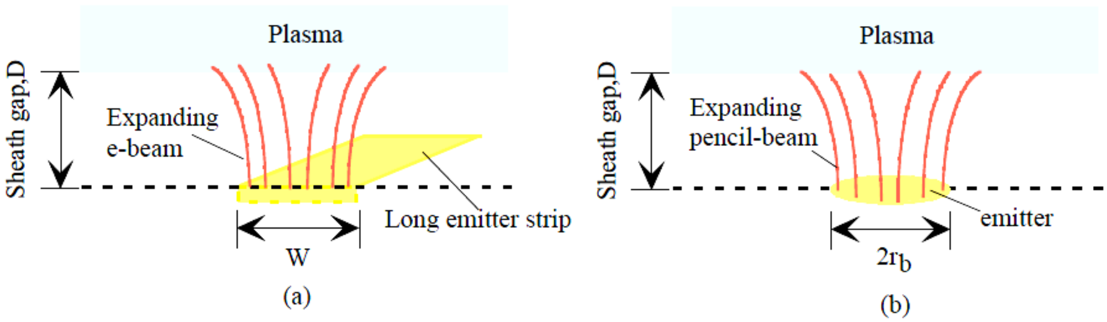

Figure 2.5 : Two and three-dimensional spreading of an emitted beam [25].

Also, at the University of Michigan, Lau extended the two-dimensional solution described above, to the two and three dimensional cases as given below

$$\frac{J_{cl}(2)}{J_{cl}(1)} = 1 + \frac{D}{4R} \quad (2.9)$$

$$\frac{J_{cl}(3)}{J_{cl}(1)} = 1 + \frac{D}{\pi W}\left(\frac{1}{4} - \frac{1}{2\pi}\right)\frac{D}{R} \quad (2.10)$$

Where, now the emitter is a planar ellipse with semi-axis R and W/2, and it is assumed that R ≥ W/2, and R/D >>1. These solutions assume a gap size and/or magnetic field, such that beam spreading is not a factor. The beam remains collimated, but the vacant expanse surrounding the beam, as opposed to the continuous charge of the one-dimensional approximation, improves the space-charge limit.

2.7 Quantum Tunneling

Quantum tunneling is a microscopic phenomenon where a particle can penetrate and in most cases pass through a potential barrier. This barrier is assumed to be higher than the kinetic energy of the particle, therefore such a motion is not allowed by the laws of classical dynamics. The simplest problems in quantum tunneling are one-dimensional and most of the research is done on these problems. But the extension of one-dimensional tunneling to higher dimensions is not straightforward. In addition there are certain characteristics that appear in two- or three-dimensional tunneling which do not show up in the one-dimensional motion.

2.7.1 History of Quantum Tunneling

Three years after the discovery of natural radioactivity in 1896, Elster and Geitel [40] found the exponential decay rate of radioactive substances experimentally. In 1900 Rutherford [41] introduced the idea of half-life of these chemicals, i.e. the time that, the number of radioactive nuclei reach on behalf of their original number. In 1905 Schweidler [42] showed the statistical nature of the decay. This means that the probability of disintegration of a nucleus does not depend on the time of its formation and also the time that a particular nucleus decays can only be predicted statistically. This idea was verified empirically by Kohlrausch in 1906. Later experiments showed that the decay width does not depend on external variables such as pressure, temperature or chemical environment. In 1930's and 1940's there were many attempts to relate the dynamics of the electron current in a system of metal-semiconductor which was used in rectifying the current, to the tunneling of electrons in solids. But the models were not realistic enough and usually quantum theory was predicting a current in the opposite direction of the observed current [43-44]. With the discovery of transistors in 1947, the tunneling of electrons received renewed attention. In 1950 the construction of semiconductors like Ge and Si had advanced to a point where it was possible to manufacture semiconductors of given characteristics. Very recently the tunneling of an individual atom, e.g. hydrogen on a metal surface, such as copper has been observed directly. A remarkable (non-classical) feature of the experiment is that the tunneling rate increases as the surface gets colder [45-46].

2.7.2 Tunneling Mechanisms

Due to constant downscaling of gate-dielectric thicknesses in modern MOS devices the effect of tunneling has drastically gained relevance. Quantum mechanical tunneling describes the transition of carriers through a classically forbidden energy state. This can be an electron tunneling from the semiconductor through a dielectric, which represents an energy barrier, to the gate contact of an MOS structure. Even if the energy barrier is higher than the electron energy, there is quantum mechanically a finite probability of this transition. The reason lies in the wavelike behavior of particles on the quantum scale where the wave function describes the probability of finding an electron at a certain position in space. As the wave function penetrates the barrier and can even extend to the other side, quantum mechanics predict a non-zero probability for an electron to be on the other side.

In the silicon-dielectric-silicon structure sketched in Figure 2.6 a variety of tunneling processes can be identified. Considering the shape of the energy barrier alone, FOWLER-NORDHEIM (FN) tunneling and direct tunneling can be distinguished. However, a more rigorous classification distinguishes between ECB (electrons from the conduction band), EVB (electrons from the valence band), HVB (holes from the valence band), and TAT (trap-assisted tunneling) processes. The EVB process is caused by electrons tunneling from the valence band to the conduction band. It thus creates free carriers at both sides of the dielectric, which, for MOS transistors, gives rise to increased substrate current. The TAT process can either be elastic, which means that the energy of the carrier is conserved, or inelastic, where the carrier loses energy due to the emission of phonons. Furthermore, in dielectrics with a very high defect density, hopping conduction via multiple defects may occur.

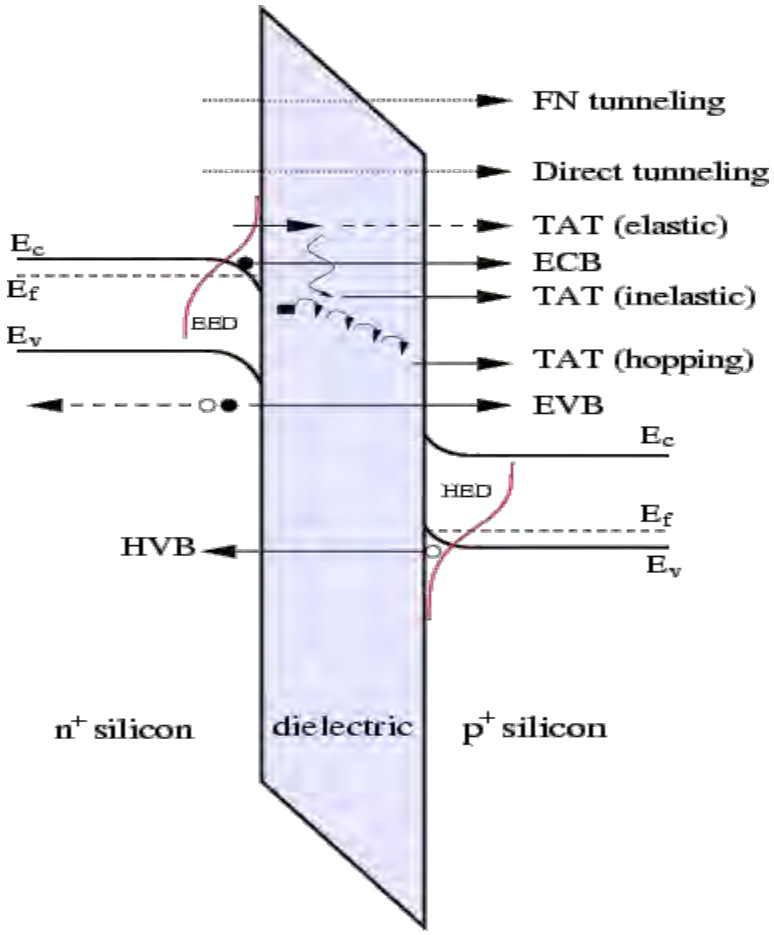

Figure 2.6: Schematic of the tunneling processes in a silicon-dielectric-silicon structure. The different tunneling processes are indicated by arrows and described in the text. The abbreviations EED and HED denote the electron and hole energy distribution function [45].

2.7.2.1 Direct Tunneling

In Figure 2.7 the energy band conditions for the direct tunneling regime are shown. Here, the electrons from the inverted silicon surface can tunnel directly through the forbidden energy barrier formed by the dielectric layer to the poly-gate. Direct tunneling is strongly gaining significance when the dielectric layer gets thinner.

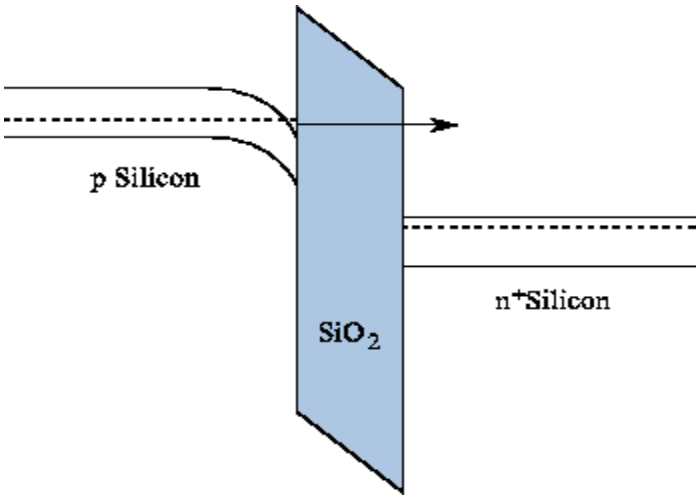

Figure 2.7 : Direct Tunneling

2.7.2.2 Fowler Nordheim Tunneling

The energy band conditions for Fowler-Nordheim tunneling, which is a special case of direct tunneling, are depicted in Figure 2.8. The electrons do not tunnel directly to the other side of the barrier. Instead they tunnel from the silicon inversion layer to the conduction band of the

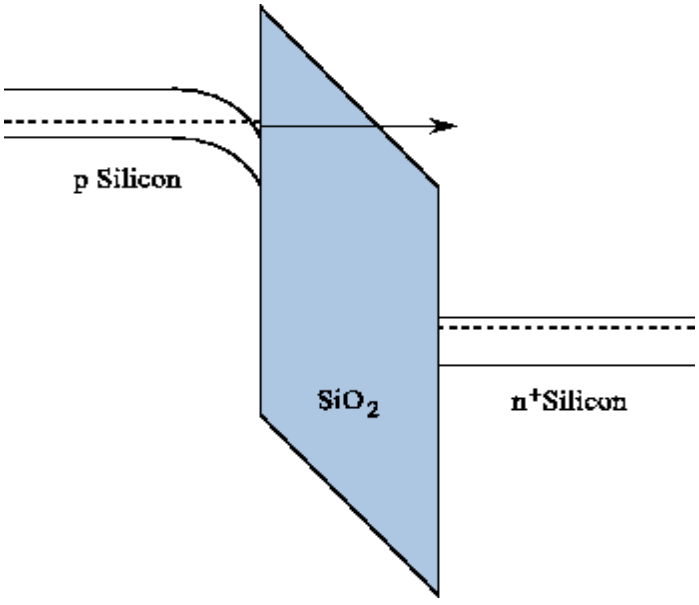

Figure 2.8 : Fowler Nordheim Tunneling

dielectric layer from where they are transported to the gate contact. The Fowler-Nordheim regime is significant for thicker dielectrics and sufficiently high electric fields.

2.7.2.3 Trap-Assisted Tunneling

As the reduction of the applied voltages does not keep up with the miniaturization of actual devices the electric fields across dielectric layers are constantly increasing. Especially for non-volatile memory cells high electric fields are necessary in order to achieve quick write and erase cycles. Due to the repeated high-field stress, defects can arise in the dielectric leading to tunneling currents, even at low fields. This stress-induced leakage current (SILC) plays a major role in the determination of the retention times of non-volatile memory cells.

2.7.2.4 Inelastic Phonon-Assisted Tunneling

The defect-assisted tunneling process of an electron from the cathode to the anode via a trap is considered as a two-step process. Electrons are captured from the cathode, relax to the energy level of the trap by emitting one or more phonons with the energy, and are then emitted to the anode. This process is inelastic as the electron energy is not conserved during the tunneling process. Figure 2.9 depicts this process including the phonon emission.

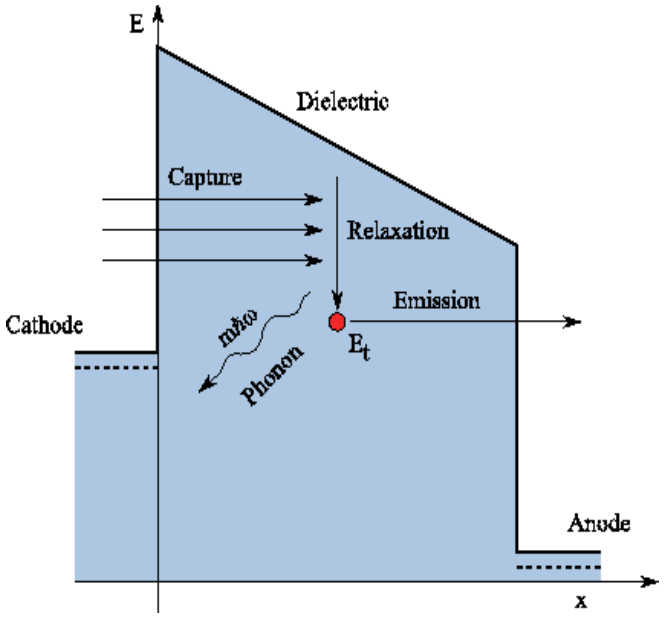

Figure 2.9 : Inelastic tunneling process including a sole trap.
The excess energy of the tunneling electron is released by means of phonon emission.

2.7.2.5 Single-Trap Assisted Tunneling

In the single-trap assisted tunneling approach the tunneling current for each trap is calculated separately. The total tunneling current is afterwards superimposed from the individual contributions. Although the interaction between neighboring traps is of importance in highly degraded dielectrics, for less degraded devices this approach can be used.

2.7.2.6 Multi-Trap Assisted Tunneling

For highly degraded devices the isolated calculation for each trap is not sufficient anymore. Anomalous charge loss in memory cells has been observed and was explained by conduction through a second trap.

2.7.3 Derivation of Fowler Nordheim Equation

The tunneling current density for an electron, passing through a general potential is derived here. The E label indicates that the vertical axis refers to the energy in the band diagram $q\phi(x)$ is the shape of the potential barrier, E_x is the electron energy along the x-direction and T_{tun} is the tunneling distance. The expression of the current density *(J)* induced by electrons tunneling in the x-direction through a generic potential barrier is

$$J = q \int_0^{\alpha} N(V_x)\, T(E_x) V_x dV_x \quad \ldots\ldots\ldots\ldots\ldots\ldots\ldots\ldots\ldots\ldots\ldots\ldots\ldots\ldots (2.10)$$

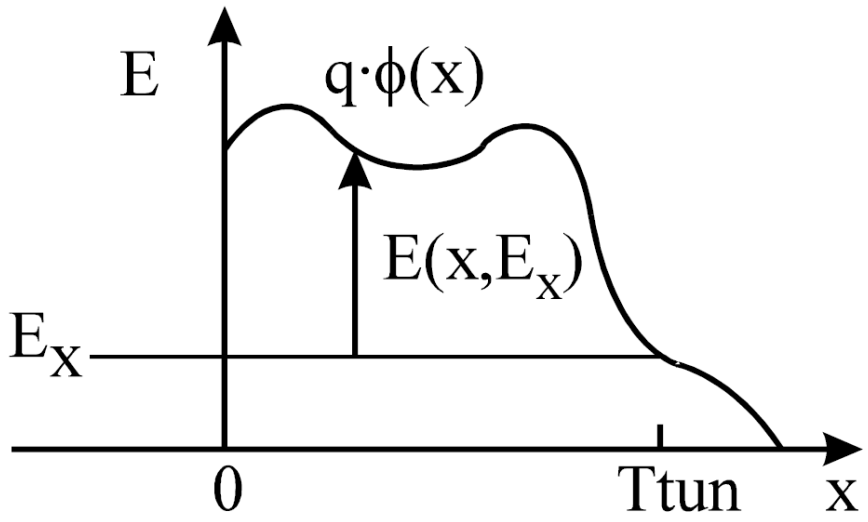

Figure 2.10 : Potential Barrier of a general shape [46].

Where, q is the charge of an individual electron, $T(E_x)$ is the tunneling probability, i.e. the probability that one electron having energy E_x along the x-axis goes through the potential barrier. $N(v_x)dv_x$ is the density of electrons with velocity between v_x and v_x+dv_x along the x-axis. The integral is taken from 0 to infinity since the electrons are trapped in the metal for x<0.

$$N(V_x) = \int_{-\alpha}^{\alpha} dv_y \int_{-\alpha}^{\alpha} dv_z \, f(\frac{1}{2}mv^2)$$

$$N(V_x) = \frac{2\pi}{m}\int_{-\alpha}^{\alpha} dE_r \, f(E_r+E_x) \dots\dots\dots\dots\dots\dots\dots\dots\dots\dots\dots (2.11)$$

Assuming that the electrons in the metal follow the free electron gas model, Pauli Exclusion Principle applies and Fermi-Dirac distribution function is introduced.

$$f\left(\frac{1}{2}mv^2\right) = \frac{1}{e^{\frac{\frac{1}{2}m\,v^2-E_f}{k_BT}}+1} \dots\dots\dots\dots\dots\dots\dots\dots\dots\dots\dots\dots (2.12)$$

The current density becomes, substituting the previous expression for $N(v_x)$ and considering the variable change $E_x = mv_x^2/2$, so that $v_xdv_x = dE_x/m$,

$$J = \frac{2\pi q}{m^2}\int_0^{\alpha} T(E_x)\, dE_x \int_{E_x}^{\alpha} f(E)\, dE$$

$$= \frac{4\pi q m k_B T}{h^3} \ln\left(e^{\frac{E_x-E_f}{k_BT}} - 1\right)\int_0^{\alpha} T(E_x)\, dE_x \dots\dots\dots\dots\dots (2.13)$$

The tunneling probability *T(Ex)* depends on the potential barrier shape and it can be calculated by the Wentzel-Kramers-Brillouin (WKB) approximation as

$$T(E_x) = e^{-2\sqrt{\frac{8\pi^2 m}{h^2}}}\int_0^{T_{tun}} \sqrt{q\phi(x)-E_x}\; dx \dots\dots\dots\dots\dots\dots\dots (2.14)$$

Where, (*q*·f*(x) – Ex)* is the difference between the energy of the potential barrier at position *x (q*·f*(x))* and the electron energy in the x-direction (*Ex*), as shown in the band diagram of Figure. After some calculation,

$$T(E_x) = T(E_f)\, e^{-2\sqrt{\frac{8\pi^2 m}{h^2}}}\left(E_f - E_x\right)\int_0^{T_{tun}} \frac{1}{\sqrt{q\phi(x)-E_x}}dx \dots\dots\dots\dots\dots (2.15)$$

Where,

$$T(E_f) = e^{-2\sqrt{\frac{8\pi^2 m}{h^2}}} \int_0^{T_{tun}} \sqrt{q\phi(x) - E_f}\, dx \ldots\ldots\ldots\ldots\ldots\ldots\ldots\ldots\ldots (2.16)$$

For a triangular potential barrier,

$$q \cdot f(x) = q \cdot f + E_f - q \cdot F \cdot x$$

$$q \cdot f - q.f.T_{tun}$$

Here, q·f(x) is the energy at point x and F is the effective electric field.

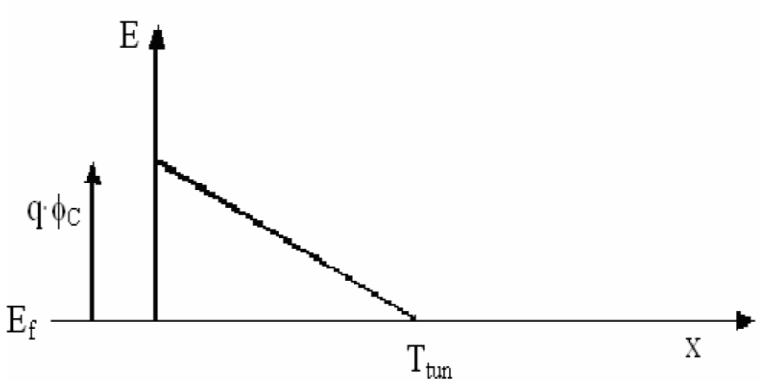

Figure 2.11 : Triangular Shape Barrier for FN Tunneling

The tunneling probability becomes

$$T(E_f) = e^{-\frac{4}{3}\sqrt{\frac{8\pi^2 m}{h^2}}\frac{(q\phi)^{\frac{3}{2}}}{qF}} \ldots\ldots\ldots\ldots\ldots\ldots\ldots\ldots\ldots\ldots\ldots (2.17)$$

Thus,

$$J = \frac{4\pi qm}{h^3}\,\frac{(k_B T)^2}{C^2}\,T(E_f)\frac{C\pi}{sinC\pi} \ldots\ldots\ldots\ldots\ldots\ldots\ldots\ldots\ldots\ldots (2.18)$$

The constant *C* becomes

$$C = k_B T\sqrt{\frac{8\pi^2 m}{h^2}}\int_0^{T_{tun}} \frac{1}{\sqrt{q\phi(x) - E_f}}dx \ldots\ldots\ldots\ldots\ldots\ldots\ldots\ldots (2.19)$$

Substituting the expressions for *T(Ef)* and *C* into the current density equation

$$J = \frac{q^2}{8\pi h\phi} F^2 e^{-\frac{4}{3}\sqrt{\frac{8\pi^2 m}{h^2}}\frac{(q\phi)^{\frac{3}{2}}}{qF}} \frac{C\pi}{sinC\pi}$$

$$\approx \frac{q^2}{8\pi h\phi} F^2 e^{-\frac{4}{3}\sqrt{\frac{8\pi^2 m}{h^2}}\frac{(q\phi)^{\frac{3}{2}}}{qF}} \ldots\ldots\ldots\ldots\ldots\ldots\ldots\ldots\ldots\ldots\ldots\ldots (2.20)$$

We can write,

$$J \approx A\frac{F^2}{\phi} e^{-\frac{B\phi^{\frac{3}{2}}}{F}} \ldots\ldots\ldots\ldots\ldots\ldots\ldots\ldots\ldots (2.21)$$

Where,

$A = 1.54 \times 10^{-6}$ & $B = 6.82 \times 10^{9}$

2.8 Future

By glancing at Table 2.1 that compares the characteristics of vacuum microelectronic devices with semiconductor devices, it becomes quite clear that, vacuum is a vastly superior transport medium compared to solids. The electron velocity in vacuum can approach the speed of light (3×10^{10} cm/s), while the saturation velocity in solid state devices is typically limited to 10^7 cm/s by collisions with optical and acoustic phonons. An electron moves ballistically in vacuum, while in solids the electronic ballistic motion is rarely sustained for more than 0.1µm, even in a two-dimensional quantum state at very low temperatures. Similarly, the coherence of electron waves in vacuum can be preserved for a long distance, while in solids it cannot be maintained further than 0.1µm. Therefore, various forms of electron-beam devices can be built by taking advantage of vacuum as the electron transport medium, and electro-optical components such as lenses, reflectors, and deflectors can also be made.

TABLE 2.1. Characteristics of Solid-State and VME Devices

Properties Solid	**State Devices**	**VME Devices**
Current density	10^4 –10^5 A/cm^2	2×10^3 A/cm^2
Voltage	>0.1 V	>10 V
Structure	Solid/solid interface	Solid/vacuum
Electron transport		
Medium	Solid	Vacuum
Ballistic	<0.1 μm, Low temp.	100% Ballistic
Coherence	Length <0.1μm *t* <10−13 s at RT	Length >> 0.1μm *t* >10−13 s
Lens effect	Difficult	Easy
Noise		
Thermal noise	Random motion of carriers	Comparable
Flicker noise	Surface/interface effects	Worse
Shot noise	Fluctuation in generation/ recombination rates of carriers	Comparable
Electron energy	<0.3eV	Several to 1000eV
Cutoff frequency	<20 GHz (Si) <100 GHz (GaAs)	<100–500 GHz
Power	Small	Large
Radiation hardness	Poor	Excellent
Temperature sensitivity	−30~50 °C	<500 °C
Fabrication/materials	Well established (Si), established (GaAs)	Not well established
Applications	Microprocessors, memory devices, optoelectronic devices, RF devices	Flat panel displays, microwave power tubes, electron/ion sources, e-beam lithography, e-beam memories and excitation devices

However, the largest current density that is ultimately achievable in FEAs is limited by space charge effects and other structural parameters, and can be estimated at about 2200 A/cm^2. In contrast, current densities in a solid-state device can be as high as $10^4 – 10^5$ A/cm2, because the equal numbers of electrons and ions in a solid-state device can neutralize the negative charge of the electrons. Vacuum devices are based on only one type of charged carrier, either negative or positive, while solid-state devices can have two carriers of opposite charges, electrons and holes. This prevents vacuum microelectronics from making energy-efficient CMOS-type devices.

For a vacuum triode, the maximum current density of FEAs will limit the cutoff frequency to less than 20 GHz based on a simple unity-current-gain frequency calculation. This limitation is due to a low transconductance that, in turn, is limited by both the capacitance and the space charge current density. The highest speed at which solid-state devices of Si and GaAs can be operated at is about 20 GHz and 100 GHz, respectively. However, if FEAs are incorporated into linear beam devices, such as klystrons, traveling wave tubes (TWT), and backward wave oscillator (BWO) tubes instead of the simple triode structure, the operating frequency of vacuum microelectronic devices can be increased to 100–500 GHz.

As far as current noise is concerned, among the three main types of noise, thermal noise, shot noise, and flicker noise, the first two types of noise are similar for both vacuum and solid-state devices. However, flicker noise is usually much greater in vacuum devices, because it originates from surface and interface effects. Under normal FEA operating conditions, it is difficult to maintain atomic stability at vacuum/solid interfaces because of complicated physical or chemical reactions such as gas adsorption, impurity migration, and ion impact. In contrast, the sources of flicker noise in solids are impurities and defects, which are relatively few and are contained inside the crystals. Fortunately, the noise from FEAs can be statistically reduced when the number of tips is greater than 1000. An extremely clean operating environment or the use of some highly stable emitting materials will also produce much lower noise.

It is important to understand that different applications call for different schemes of optimization for device characteristics. For flat panel display applications, the current density rarely needs to exceed more than 0.01 A/cm^2. Instead, it is more essential to find a low cost solution to uniformly produce large area FEAs that can be operated at low voltages. In this regard, the recent trend of exploring new cathode materials, such as carbon-based emitters is encouraging. It is conceivable that FEDs, owning to their inherent advantages of brighter image, wider viewing

angle, less energy consumption, and higher resolution, will someday be able to compete effectively with liquid crystal displays and other technologies in the flat panel display market. It is also probably vital for the future of this technology that researchers look beyond the current display and microwave devices and start to think about next generation, functional ―beam" devices for memory, switching, and other applications. Only by doing so, we will be able to allow the unique capability of vacuum microelectronics in creating ―beam" devices to complement solid-state technology in bringing further advanced products to the marketplace.

Chapter 3

Analytical Modeling of VFET

3.1 Introduction

To address the problem of designing and evaluating a vacuum device like VFET, a concise model of the device is the ultimate tool to explain the characteristics of the device. This concise model allows making future projections of the device performance under different conditions. So far, no significant work has been done in this respect. A concise model can be very complex to accommodate all the underlying device physics basic which can be extrapolated for scaled device and for fast circuit optimization. On the other hand, a simplified model allows different simplifications to offer a fast analysis of device behavior. The model to represent the device behavior is dependent on electrode numbers and types.

3.2 Threshold Voltage

The threshold voltage, commonly abbreviated as V_{th} or $V_{GS\,(th)}$, of a field-effect transistor (FET) is the minimum gate-to-source voltage differential that is needed to create a conducting path between the source and drain terminals.

At gate-to-source voltages above the threshold voltage ($(V_{GS} > V_{th})$ but still below saturation (less than "fully on", $(V_{GS} - V_{th}) > V_{DS}$), the transistor is in its 'linear region', also known as ohmic mode, where it behaves like a voltage-controlled variable resistor.

When referring to a junction field-effect transistor (JFET), the threshold voltage is often called "pinch-off voltage" instead. This is somewhat confusing since "pinch off" applied to insulated-gate field-effect transistor (IGFET) refers to the channel pinching that leads to current saturation behavior under high source–drain bias, even though the current is never off. Unlike "pinch off", the term "threshold voltage" is unambiguous and refers to the same concept in any field-effect transistor.

In n-channel enhancement-mode devices, a conductive channel does not exist naturally within the transistor, and a positive gate-to-source voltage is necessary to create one. The positive voltage attracts free-floating electrons within the body towards the gate, forming a conductive channel. But first, enough electrons must be attracted near the gate to counter the dopant ions added to the body of the FET; this forms a region with no mobile carriers called a depletion region, and the voltage at which this occurs is the threshold voltage of the FET. Further gate-to-source voltage increase will attract even more electrons towards the gate which are able to create a conductive channel from source to drain; this process is called inversion.

In contrast, n-channel depletion-mode devices have a conductive channel naturally existing within the transistor. Accordingly, the term 'threshold voltage' does not readily apply to turn such devices 'on', but is used instead to denote the voltage level at which the channel is wide enough to allow electrons to flow easily. This ease-of-flow threshold also applies to p-channel depletion-mode devices, in which a positive voltage from gate to body/source creates a depletion layer by forcing the positively charged holes away from the gate-insulator/semiconductor interface, leaving exposed a carrier-free region of immobile, negatively charged acceptor ions.

In wide planar transistors the threshold voltage is essentially independent of the drain–source voltage and is therefore a well defined characteristics; however, it is less clear in modern nanometer-sized MOSFETs due to drain-induced barrier lowering.

If the gate voltage is below the threshold voltage, the transistor is turned off and ideally there is no current from the drain to the source of the transistor. In fact, there is a current even for gate biases below the threshold (sub-threshold leakage) current, although it is small and varies exponentially with gate bias.

If the gate voltage is above the threshold voltage, the transistor is turned on, due to there being many electrons in the channel at the oxide-silicon interface, creating a low-resistance channel where charge can flow from drain to source. For voltages significantly above the threshold, this situation is called strong inversion. The channel is tapered when $V_D > 0$ because the voltage drop due to the current in the resistive channel reduces the oxide field supporting the channel as the drain is approached.

In VFET, the threshold condition is somewhat different, as the channel is vacuum. The electron flow through a metal nano-gap structure usually involves 2 steps process :

1. Child-Langmuir SCL current flow
2. Fowler Nordheim field emission (Tunneling)

SCL regime seems to appear at very low drain voltages (~0.5V), which is not the case for FN regime. The voltage range tested for Fowler Nordheim regime is above 2V for an anode to cathode distance of ~ 100nm and sharp cathode tip. The pre-requisite for a substantial current flow is a surface normal field of significant strength (order of $10V\mu m^{-1}$ for metals with work function of 4-5 eV). This surface field accumulates charges in cathode near the tip region. So, we can say in other words that, the ON current of the transistor requires certain accumulation charges at cathode tip. The minimum gate voltage which accumulates this amount charges i.e. provides that minimum surface normal field would be the threshold voltage for VFET.

3.2.1 Modeling of Threshold Voltage in VFET

The cross section of a VFET is shown in Figure 3.1 with different structural parameters of the device. The parameters are

Q = Total charge confined in the source / cathode

L = Length from the bottom of cathode to anode (d + h)

r_c = Channel radius

r_{in} = Cathode tip radius

r_{out} = distance from outer side of cathode tip to channel radius

d = Anode to cathode distance

h = Cathode tip height

W_g = Gate Width

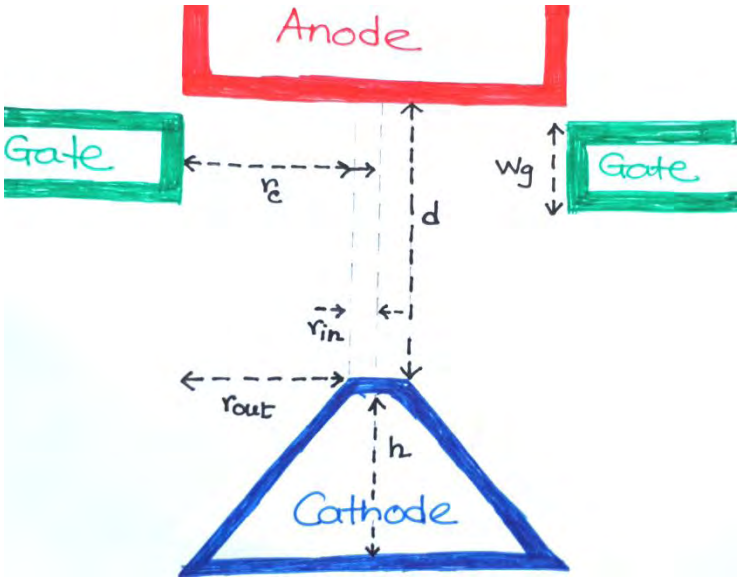

Figure 3.1 : Cross section of a VFET showing different structural parameters

Electric field through the nano-void channel can be given by,

$$\boldsymbol{E} = \boldsymbol{a}\frac{Q}{2\pi\varepsilon L r_c} \ldots\ldots\ldots\ldots\ldots\ldots\ldots\ldots\ldots\ldots\ldots\ldots\ldots\ldots\ldots\ldots\ldots\ldots (3.1)$$

The value of the electric field,

$$|E| = \frac{Q}{2\pi\varepsilon(d+h)r_c} \ldots\ldots\ldots\ldots\ldots\ldots\ldots\ldots\ldots\ldots\ldots\ldots\ldots\ldots\ldots\ldots\ldots\ldots (3.2)$$

Minimum accumulation charge required in cathode to reach channel on the verge of conduction,

$$Q_{acc} = |E_{min}|2\pi\varepsilon(d+h)r_c \ldots\ldots\ldots\ldots\ldots\ldots\ldots\ldots\ldots\ldots\ldots\ldots\ldots\ldots\ldots\ldots\ldots\ldots (3.3)$$

Where,

$|E_{min}|$ = Minimum electric field for channel formation

Assuming, the gate and cathode as a coaxial cylindrical structure, potential difference between gate and cathode, while minimum charge is accumulated

$$V = -\int_{r_{out}}^{r_{in}} E.dl$$

$$= -\int_{r_{out}}^{r_{in}} \frac{Q_{acc}}{2\pi\varepsilon W_g r} dr$$

$$= -\frac{Q_{acc}}{2\pi\varepsilon W_g} \int_{r_{out}}^{r_{in}} \frac{dr}{r}$$

$$= -\frac{Q_{acc}}{2\pi\varepsilon W_g} [\ln(r)]_{r_{out}}^{r_{in}}$$

$$= -\frac{Q_{acc}}{2\pi\varepsilon W_g} \left[\ln \frac{r_{in}}{r_{out}}\right] \ldots\ldots\ldots\ldots\ldots\ldots\ldots\ldots\ldots\ldots\ldots\ldots\ldots\ldots\ldots\ldots\ldots\ldots\ldots\ldots\ldots\ldots\ldots\ldots\ldots\ldots\ldots\ldots. (3.4)$$

Here,

r_{in} = cathode tip radius

r_{out} = distance from outer side of cathode tip to channel radius

We assumed the structure as a coaxial cylindrical one. But actually it is not, as the cathode shape is conical, a non-uniform conical to be exact. So we have to incorporate this to compensate for our assumption. Hence a structure dependent parameter ‗c' has been introduced. Incorporating the non uniform geometric structure of the cathode, the threshold voltage can be given by equation (3.5)

$$V_{th} = \frac{Q_{acc}}{2\pi\varepsilon W_g} \left[\ln \frac{cr_{in}}{r_{out}}\right] \ldots\ldots\ldots\ldots\ldots\ldots\ldots\ldots\ldots\ldots\ldots\ldots\ldots\ldots (3.5)$$

Replacing from equation (3.3),

$$V_{th} = \frac{|E_{min}|(d+h)r_c}{W_g} \left[\ln \frac{cr_{in}}{r_{out}}\right] \ldots\ldots\ldots\ldots\ldots\ldots\ldots\ldots\ldots\ldots\ldots\ldots (3.6)$$

3.3 Drive in Voltage

Overdrive voltage, usually abbreviated as V_{OV}, is typically referred to in the context of MOSFET transistors. The overdrive voltage is defined as the voltage between transistor gate and source (V_{GS}) in excess of the threshold voltage (V_{th}) where V_{th} is defined as the minimum voltage required between gate and source to turn the transistor on (allow it to conduct

electricity). Due to this definition, overdrive voltage is also known as "excess gate voltage" or "effective voltage." Overdrive voltage can be found using the simple equation: $V_{OV} = V_{GS} - V_{th}$.

As has been stated earlier, in VFET, current flow involves two regimes; Space charge limited current and Fowler Nordheim tunneling current. SCL regime seems to appear at very low drain voltages (~0.5V). The drain voltage literally breaks free the carriers (electron) from the cathode tip, thus causes the ballistic transport in vacuum. The minimum voltage at drain that starts the SCL regime (a current density of 10^5 Acm^{-2}) can be defined as drive in voltage of VFET. The derivation of drive in voltage is done in the next section using the space charge limited emission theory.

3.3.1 Modeling of Drive in Voltage in VFET

Current density for space charge limited emission,

$$J_{SCL} = \frac{4}{9}\,\varepsilon\sqrt{\frac{2e}{m}}\,\frac{V^{\frac{3}{2}}}{D^2}$$

$$= \frac{4}{9}\,\varepsilon\sqrt{\frac{2e}{m}}\left(\frac{V}{D}\right)^2\frac{1}{\sqrt{V}}$$

$$= \frac{4}{9}\,\varepsilon\sqrt{\frac{2e}{m}}\,(E)^2\frac{1}{\sqrt{V}} \ldots\ldots\ldots\ldots\ldots\ldots\ldots\ldots\ldots\ldots\ldots\ldots (3.7)$$

Effective electric field,

$$E_{eff} = \beta V_A \ldots\ldots\ldots\ldots\ldots\ldots\ldots\ldots\ldots\ldots\ldots\ldots\ldots\ldots\ldots\ldots (3.8)$$

Here, V_A = Applied anode voltage

Replacing in equation (3.7)

$$J_{SCL} = \frac{4}{9}\,\varepsilon\sqrt{\frac{2e}{m}}\,(\beta V_A)^2\frac{1}{\sqrt{V_A}} \ldots\ldots\ldots\ldots\ldots\ldots\ldots\ldots\ldots\ldots\ldots\ldots\ldots (3.9)$$

Drive in voltage (V_{AD}) is the minimum anode voltage while device has the off current (J_{min}). Placing these in equation (3.9),

$$J_{min} = \frac{4}{9}\,\varepsilon\sqrt{\frac{2e}{m}}\,(\beta V_{AD})^2\frac{1}{\sqrt{V_{AD}}} \quad \ldots\ldots\ldots\ldots\ldots\ldots\ldots\ldots\ldots\ldots (3.10)$$

After some calculation,

$$(V_{AD})^{-\frac{3}{2}} = \frac{4}{9}\,\varepsilon\sqrt{\frac{2e}{m}}\,(\beta)^2\frac{1}{J_{min}} \quad \ldots\ldots\ldots\ldots\ldots\ldots\ldots\ldots\ldots\ldots (3.11)$$

So, the drive in voltage can be given by

$$V_{AD} = \left(\frac{4}{9}\,\varepsilon\sqrt{\frac{2e}{m}}\,(\beta)^2\frac{1}{J_{min}}\right)^{-\frac{2}{3}} \quad \ldots\ldots\ldots\ldots\ldots\ldots\ldots\ldots\ldots\ldots (3.12)$$

3.4 Effective Electric Field

Classical field emission is described by the Fowler– Nordheim (FN) theory for the case of an isotropic material where the tip geometry is treated in a planar approximation and the applied electric field is a constant throughout free space and at the surface of the emitter. This effective parallel plate approximation for the electric field at the emitter surface has been successfully applied in the past to electrochemically etched, refractory metal emitters with radii of curvature on the order of 50–100 nm. It is common practice in analyzing the performance of field emission microtips or arrays (FEA) to adapt the one-dimensional (1D) FN equation to cases of atomically sharp and nearly atomically sharp, three-dimensional (3D) field emission structures [47].

The calculation of the tunneling current requires knowledge of the electric field at the emitter surface, a quantity that the classical FN analysis presumes to be constant due to the 1D nature of the derivation. It is evident that for 3D emission structures composed of microtips with radius of curvature on the order of 10 nm or less, the magnitude of the electric field is greatest at the region of greatest surface variation (the apex) and decays rapidly with increasing surface distance from the apex. Consequently, the extension of the FN theory to an inherently 3D

structure, such as a microtip, requires an exact 3D solution for the electric potential both at the emitter surface and in the adjoining free space region between the emitter and anode.

3.4.1 Field Enhancement Factor

Characteristic of conducting objects at electrostatic equilibrium is that the electric fields are strongest at locations along the surface where the object is most curved. The curvature of a surface can range from absolute flatness on one extreme to being curved to a*blunt* point on the other extreme. A flat location has no curvature and is characterized by relatively weak electric fields. On the other hand, a *sharp point* has a high degree of curvature and is characterized by relatively strong electric fields. A sphere is uniformly shaped with the same curvature at every location along its surface. As such, the electric field strength on the surface of a sphere is everywhere the same.

An empirical approach widely used to adapt the 1D FN analysis to inherently 3D structures is to model the surface electric field as some constant times the applied voltage V (i.e., $F = \beta V$), where ‗β' is commonly called the ‗‗field enhancement factor'' and is a function of the tip geometry. For example, simplest model for the field enhancement factor is

$$\beta = \frac{1}{kr} \ldots\ldots\ldots\ldots\ldots\ldots\ldots\ldots\ldots\ldots\ldots\ldots\ldots\ldots\ldots\ldots\ldots . (3.13)$$

Where, r is the microtip radius of curvature and k is a factor to be determined experimentally [48]. The b factors are routinely used and provide reasonable fits to current and voltage data. The presence of a gate potential introduces another empirically determined factor. Similarly, an area factor, given by the ratio of the tip current to the current density, is introduced and often, but erroneously, treated as constant. The correct estimation of emission area includes some subtlety [49], described in a later portion of this chapter.

Theoretical difficulties for the field enhancement factor are known to arise in the context of extremely sharp tips (tip radius r < 10 nm) [50]. For example, the FN analysis has built-in assumptions concerning the electron supply function and induced surface charge; assumptions that are predicated on a planar, semi-infinite medium emission surface. For the case of extremely sharp tips, either the radius of curvature or the physical dimension of the tip may violate such

assumptions. An additional, conceptual difficulty with the field enhancement approach is that generally the electric field is treated as a constant over the entire emission surface. Early efforts to analytically model such variation in b treated the apex of the microtip as a floating sphere [51]. The principal difficulty of utilizing the field enhancement concept in experimental analysis is that in the FN equation, ‗β' often is conjoined with the work function ‗ϕ', the estimate of which is complicated by crystal planes and the presence of adsorbates and oxides.

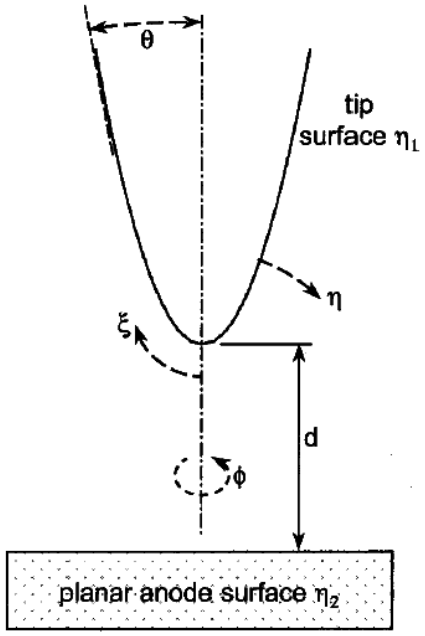

Figure 3.2 : Spheroidal Co-ordinate System at Cathode Tip [53]

The variation in the strength of the electric field along the microtip surface is a function of the applied voltage, distance from the tip apex, and the coupled, geometric factors of tip radius ‗r' and tip half-angle ‗θ'. This tip geometry and position dependence for the electric field is expressed by ‗k'. The sharpness of the tip, as determined by the tip half angle ‗θ', can vary from 0 to π/2, with θ ⇒ π/2 refers a flat surface, and θ ⇒ 0 refers a sharp point. Using the microtip geometric relationship $\cos^2\theta = d / (d+r)$, the asymptotic limits of the above equation are given by

$$k = \begin{cases} \frac{1}{2}\ln\left(\frac{4d}{r}\right) \dots\dots r \ll d \\ \frac{d}{r} \qquad \dots\dots\dots r > d \end{cases} \dots\dots\dots\dots\dots\dots\dots\dots\dots\dots\dots\dots\dots\dots (3.14)$$

3.4.2 Modeling Effective Electric Field

Electric field at the cathode tip of VFET has contribution from both gate and anode voltages. Both components referred by Figure 3.3 can be summed up and written as,

$$F_0 = \frac{V_{ds}}{d} + \frac{2V_{gs}}{\sqrt{r_c{}^2 + d^2}} cos\theta \quad \ldots\ldots\ldots\ldots\ldots\ldots\ldots\ldots\ldots\ldots\ldots\ldots\ldots\ldots (3.15)$$

Where,

$$\text{Angle, } \theta = \tan^{-1}\frac{r_c}{d} \quad \ldots\ldots\ldots\ldots\ldots\ldots\ldots\ldots\ldots\ldots\ldots\ldots\ldots\ldots\ldots\ldots\ldots\ldots (3.16)$$

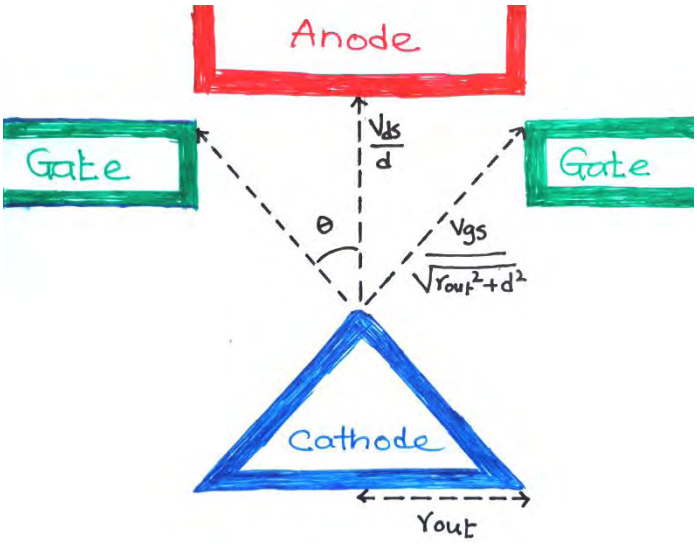

Figure 3.3 : Electric field through void channel of VFET

For, a higher anode-cathode distance and channel radius i.e. cathode radius field component due to gate voltage gets negligible. To find the effective field we have to multiply potential distribution due to electric field (equation (3.15)) by field enhancement factor.

The effective electric field,

$$F = \beta V(F_0) \quad \ldots\ldots\ldots\ldots\ldots\ldots\ldots\ldots\ldots\ldots\ldots\ldots\ldots\ldots\ldots\ldots\ldots\ldots (3.17)$$

Where, field enhancement factor,

$$\beta = \frac{1}{kr}$$

And,

$$k = \begin{cases} \frac{1}{2}\ln\left(\frac{4d}{r}\right) \dots\dots r \ll d \\ \frac{d}{r} \quad \dots\dots\dots r > d \end{cases}$$

3.5 Effective Emission Area

The emission area is supposed to be the tip area of the cathode. But in practical, the whole tip area is not engaged in emission. The effective emission area is reduced due to the angular dependence of the regular fields [52].

Effective emitting area,

$$S = 2\pi \mathrm{r_{in}}^2 \frac{F^2}{\gamma_{\mathrm{F}} \beta F_0} \dots\dots\dots\dots\dots\dots\dots\dots\dots\dots\dots\dots\dots\dots\dots\dots (3.18)$$

Where, the field can be given by

$$F \approx \beta F_0$$

So,

$$S = 2\pi \mathrm{r_{in}}^2 \frac{\beta F_0}{\gamma \mathrm{F}} \dots\dots\dots\dots\dots\dots\dots\dots\dots\dots\dots\dots\dots\dots\dots\dots\dots (3.19)$$

Here,

$\mathrm{r_{in}}$ = Cathode tip radius

F_0 = Applied electric field

β = Field Enhancement Factor

γ = 0.66

And

$$\mathfrak{f} = \frac{2\pi}{3eh}\ 4\sqrt{2m}\phi^{\frac{3}{2}} \ldots\ldots\ldots\ldots\ldots\ldots\ldots\ldots\ldots\ldots\ldots\ldots\ldots\ldots (3.20)$$

m = Electron mass

ϕ = Work function of emitting material

The maximum emission angle ranges from 10° to 25° for a gate voltage of 10V gives an energy spread of 1eV [53]. A successful emission and transmission both are required for anode to cathode current. Thus, we can conclude about the effective emission area,

$$S = 2\pi \mathrm{r_{in}}^2 \frac{\beta F_0}{\gamma \mathfrak{f}} \frac{2\theta}{180} \ldots\ldots\ldots\ldots\ldots\ldots\ldots\ldots\ldots\ldots\ldots\ldots\ldots\ldots\ldots\ldots (3.21)$$

Where, $\theta = 10°$ to $25°$.

3.6 Overall Drain/Anode to Source/Cathode Current Equation

As stated earlier, the electron flow through a metal nano-gap structure usually involves a two step process: field emission from the metal surface, commonly described by Fowler–Nordheim theory, and subsequent transport through the gap, governed by Child–Langmuir SCL current flow. The Child–Langmuir law assumes zero normal field at the cathode surface, whereas Fowler–Nordheim emission requires a surface-normal field of significant strength (typically of the order of 10 $V\mu m^{-1}$ for metals with a work function of 4–5 eV) to enable tunneling emission through the potential barrier at the cathode. Usually, SCL regime begins to appear at very low voltages (<0.5 V), but the Fowler– Nordheim regime is absent in the voltage range < 2 V. This observation is consistent with earlier researches [54] that the barrier height for electrons at cathode edges is very low. In the 2DES with net accumulation charges, electron emission from the cathode edges is virtually thresholdless, enabling very low-voltage operation (similar to the negative electron affinity effect) of channel transport with high current density. Similarly, electrons approaching the anode edges will experience Coulombic attraction from the two-dimensional hole system formed there, and this will help in the capture of electrons by the anode. The different voltage dependences of the two regimes (Fowler–Nordheim versus 2DES-enabled

SCL) were confirmed in a different experiment [55]. Unlike conventional cold cathodes, the nano-void channel structure also demonstrates good stability and endurance in electron emission. So the total current density,

$$J = J_t + J_{SCL}$$

$$= \mathrm{A}\frac{\mathrm{F}^2}{\phi}\mathrm{e}^{-\frac{\mathrm{B}\phi^{\frac{3}{2}}}{\mathrm{F}}} + \frac{4}{9}\,\varepsilon\sqrt{\frac{2e}{m}}\,\beta^2(V_A - V_{AD})^{\frac{3}{2}} \ldots\ldots\ldots\ldots\ldots\ldots\ldots\ldots (3.22)$$

Where, effective electric field

$$F = \beta V$$

So, channel current

$$I = JS$$

Where, effective emission area

$$S = 2\pi \mathrm{r_{in}}^2 \frac{\beta F_0}{\gamma_\mathrm{F}} \frac{2\theta}{180}$$

So, final expression for channel current,

$$I = \left\{ \mathrm{A}\frac{\mathrm{F}^2}{\phi}\mathrm{e}^{-\frac{\mathrm{B}\phi^{\frac{3}{2}}}{\mathrm{F}}} + \frac{4}{9}\,\varepsilon\sqrt{\frac{2e}{m}}\,\beta^2(V_A - V_{AD})^{\frac{3}{2}} \right\} \left(2\pi \mathrm{r_{in}}^2 \frac{\beta F_0}{\gamma_\mathrm{F}} \frac{2\theta}{180} \right) \ldots\ldots\ldots\ldots (3.23)$$

3.7 Summary

The advantages of a vacuum tube and solid state transistors were combined in a nanoscale vacuum transistor (VFET). Our proposed model provides the opportunity to evaluate the vacuum device characteristics and determine the future projections as well. It shows good conformity with the simulation data available. With some modifications for cathode efficiency, this analytical model will provide greater accuracy.

Chapter 4

Results and Discussion

4.1 Introduction

This chapter depicts the numerical verification of our proposed model for VFET (Vacuum Field Effect Transistor). The numerical analysis i.e. the simulation of the analytical model has been done in MATLAB. After that, these have been verified with the practical work i.e. fabricated device data of different parameters (Channel current [1,8], Threshold Voltage [7], etc.) available. We will see that, proposed model shows pretty much conformity with the actual simulation data.

4.2 Threshold Voltage

Our proposed model for the threshold voltage of VFET was

$$V_{th} = \frac{|E_{min}|(d+h)r_c}{W_g}[\ln\frac{\mathrm{kr_{in}}}{\mathrm{r_{out}}}]$$

We see that, it is a function of the anode to cathode distance (d) and cathode tip radius (r_{in}). As discussed in previous chapter, this is the minimum gate voltage that provides minimum surface normal field and accumulates charges at cathode tip. Gate voltage over threshold causes onset of Fowler Nordheim emission.

4.2.1 Varying Anode to Cathode Distance

Figure 4.1 shows threshold voltage of VFET as a function of anode to cathode gap. Threshold voltage increases with the increase of the gap length as carriers have to cross a wider band. We see that, the analytical model matches the simulation data more when the anode-cathode distance is lower. The percentage of error of the analytical model is higher for longer channel. It can be explained, as longer channel involves in much leakage current [1]. Thus the minimum accumulation charges required would be greater as is the threshold voltage.

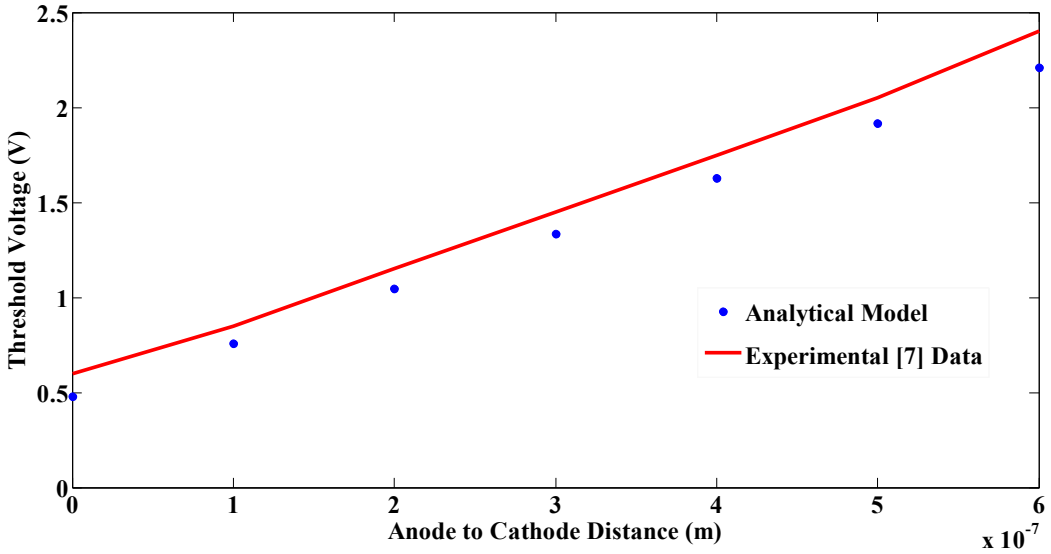

Figure 4.1 : Threshold Voltage as a function of Anode to Cathode Gap with a tip radius of 5 nm.

4.2.2 Varying Cathode Tip Radius

Figure 4.2 shows threshold voltage of VFET as a function of cathode tip radius. Increase in tip radius results an increase in threshold voltage due to the field enhancement phenomena as discussed in previous chapter.

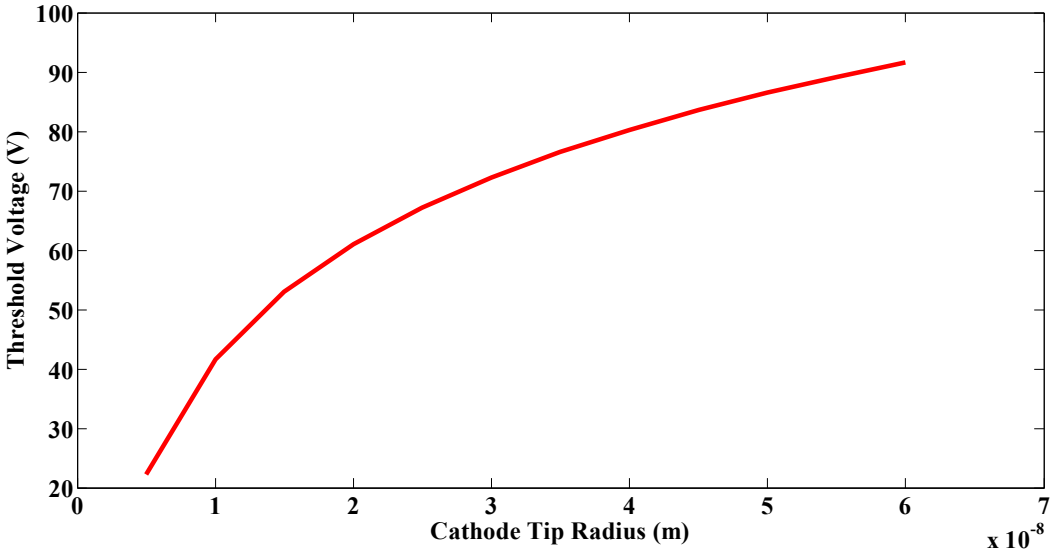

Figure 4.2 : Threshold Voltage as a function of cathode tip Radius with an Anode to Cathode Gap of 3µm.

4.3 Drive in Voltage

Drive in voltage is the minimum voltage at drain that starts the SCL regime (a current density of 10^5 Acm^{-2}). The analytical model for drive in voltage for VFET has been derived as

$$V_{AD} = \left(\frac{4}{9} \varepsilon \sqrt{\frac{2e}{m}} (\beta)^2 \frac{1}{J_{min}} \right)^{-\frac{2}{3}}$$

We see that, it is a function of field enhancement factor β, which itself is a function of anode to cathode distance (d) and cathode tip radius (r).

$$\beta = 1/kr$$

Where,

$$k = \begin{cases} \frac{1}{2} \ln\left(\frac{4d}{r}\right) \ldots\ldots r \ll d \\ \frac{d}{r} \quad \ldots\ldots\ldots r > d \end{cases}$$

Figure 4.3 shows drive in voltage of VFET as a function of anode to cathode gap. Increase in anode-cathode distance results increase in drive in voltage.

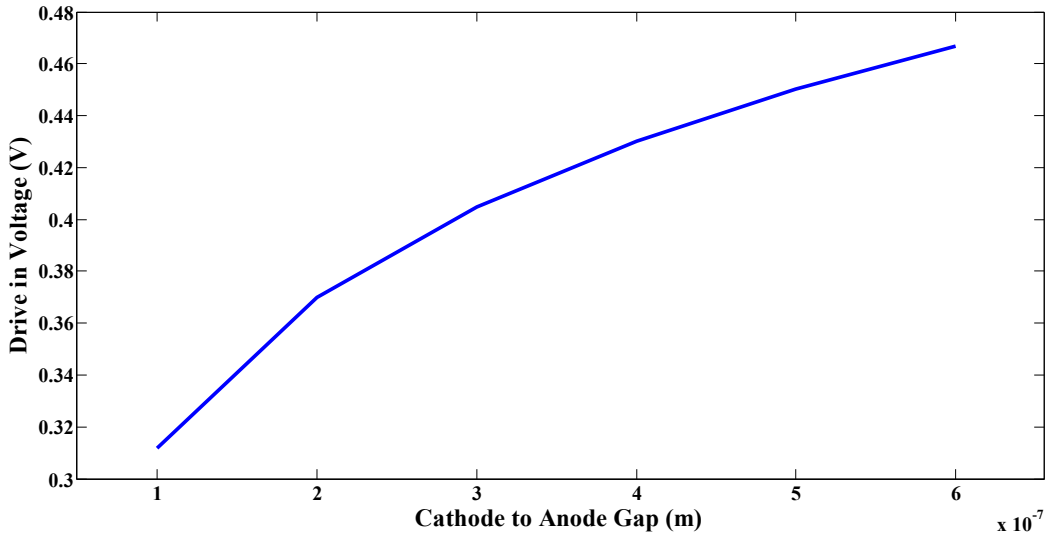

Figure 4.3 : Drive in Voltage as a function of Anode to Cathode Gap with a tip radius of 5 nm.

4.4 Space Charge Limited Current

SCL current suggests a scattering free ballistic transport of electron across a gap with low barrier height for carrier injection. Space charge limited current is given by the following equation,

$$J_{SCL} = \frac{4}{9}\varepsilon\sqrt{\frac{2e}{m}}\frac{V^{\frac{3}{2}}}{D^2}$$

Figure 4.4 shows the SCL current density as a function of drain / anode voltage. It has $V^{\frac{3}{2}}$ dependence as in the equation.

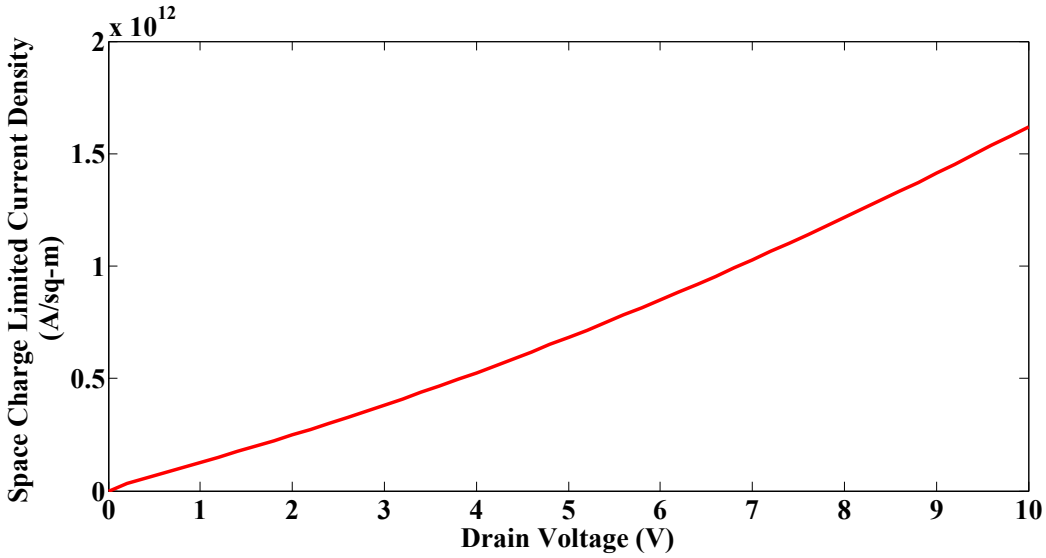

Figure 4.4: Space Charge Limited Current Density vs. Drain/Anode Voltage.
For Anode to Cathode Gap of 100 nm and Tip Radius of 5 nm.

4.5 Tunneling Current

Derivation of Fowler Nordheim tunneling current density equation has been shown in chapter 3. The current density is given by the equation

$$J \approx A\frac{F^2}{\phi}e^{-\frac{B\phi^{\frac{3}{2}}}{F}}$$

Figure 4.5 shows the FN tunneling current density as a function of drain / anode voltage. Increase in field force with the increase of drain voltage results current density increase.

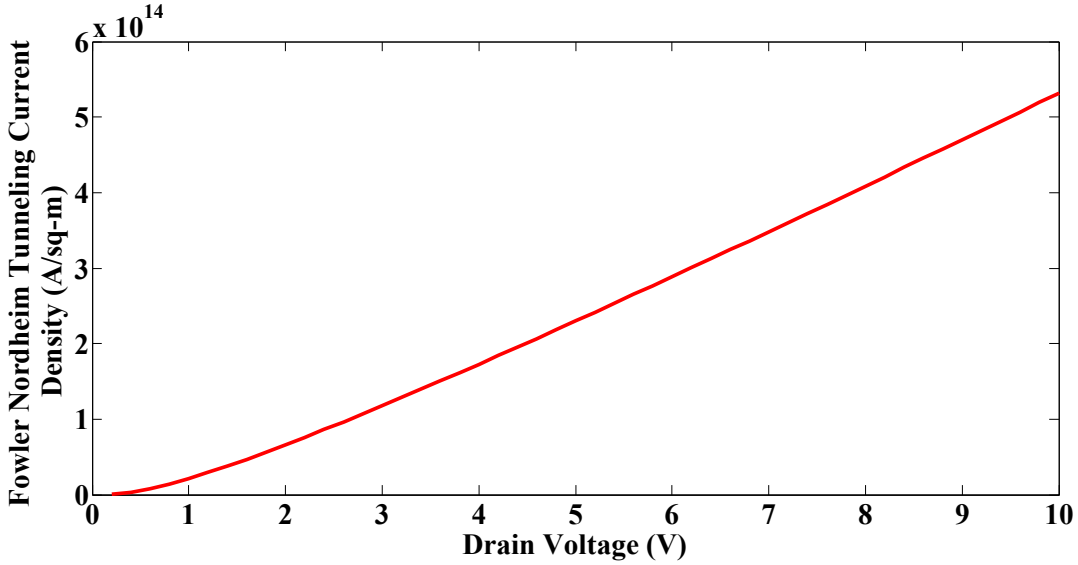

Figure 4.5 : Fowler Nordheim Tunneling Current Density vs. Drain/Anode Voltage. For Anode to Cathode Gap of 100 nm and Tip Radius of 5 nm.

4.6 Total Channel Current

Combining the two current density components we have the total current density,

$$J = J_t + J_{SCL}$$

$$= \mathrm{A}\frac{\mathrm{F}^2}{\phi}\mathrm{e}^{-\frac{\mathrm{B}\phi^{\frac{3}{2}}}{\mathrm{F}}} + \frac{4}{9}\,\varepsilon\sqrt{\frac{2e}{m}}\,\beta^2(V_A - V_{AD})^{\frac{3}{2}}$$

Incorporating the effective emission area we have the channel current as stated in previous chapter,

$$I = \left\{ \mathrm{A}\frac{\mathrm{F}^2}{\phi}\mathrm{e}^{-\frac{\mathrm{B}\phi^{\frac{3}{2}}}{\mathrm{F}}} + \frac{4}{9}\,\varepsilon\sqrt{\frac{2e}{m}}\,\beta^2(V_A - V_{AD})^{\frac{3}{2}} \right\}\left(2\pi R^2\frac{\beta F_0}{\gamma_{\mathrm{F}}}\frac{2\theta}{180}\right)$$

Figure 4.6 & 4.7 shows channel current as a function of drain voltage for a gate voltage of 2V and 6V respectively. Both the analytical model and simulation data obtained from [8] have been plotted here. There is mismatch between the plots and the deviation of the analytical model from the simulated one is increasing with the increase of drain voltage. The explanation of this deviation is that, in the simulation data or the real time data the cathode efficiency has a big deal. With the increase of drain voltage and current cathode tips get hotter and cathode tip may not be

as sharp as it was at start. This might effects parameters like threshold and drive in voltage. The temperature issue has viable significance on the performance of the cathode. Thus it can‘t be said that, the efficiency of the cathode was same all along the simulation voltage range from 1V to 10V.

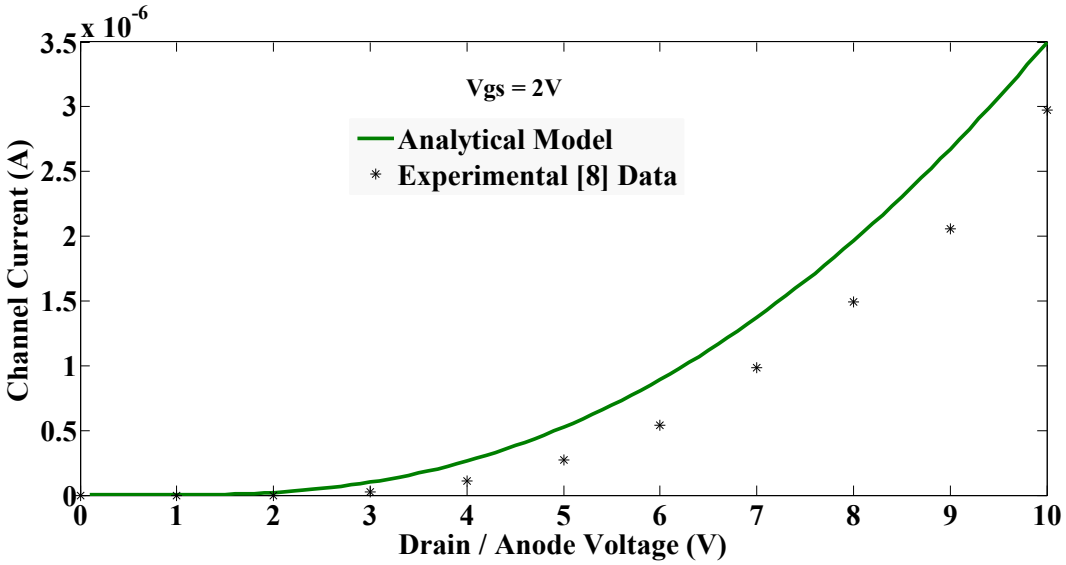

Figure 4.6 : Channel Current vs. Drain/Anode Voltage with Vgs at 2V.
For Anode to Cathode Gap of 100 nm and Tip Radius of 5 nm.

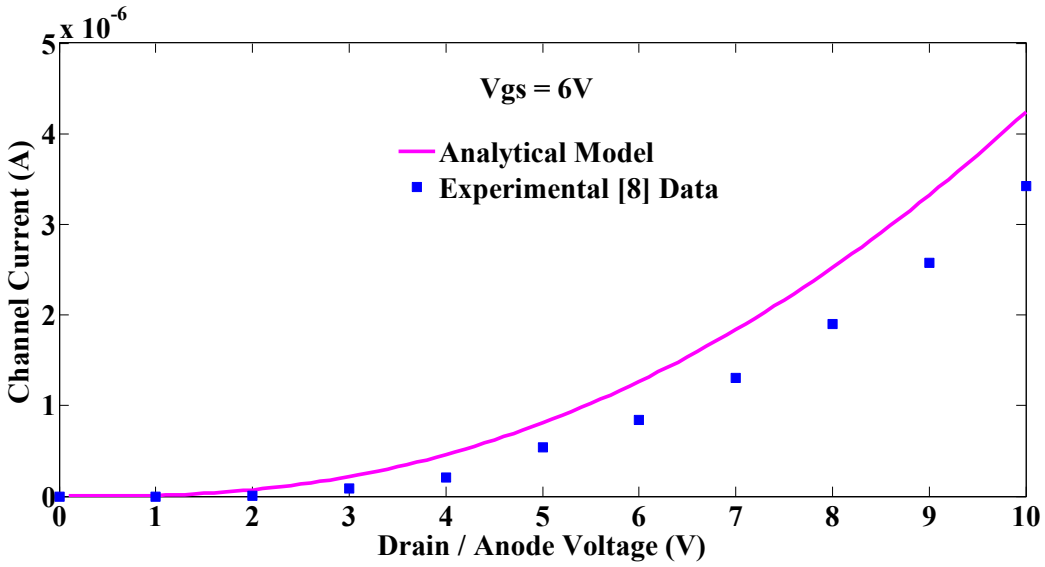

Figure 4.7 : Channel Current vs. Drain/Anode Voltage with Vgs at 6V.
For Anode to Cathode Gap of 100 nm and Tip Radius of 5 nm.

Besides this deviation, our proposed model shows enough conformity with the actual data. The solution of the deviation can be including a temperature dependent efficiency factor in our model which will incorporate the efficiency degradation with increase of drain current and voltage.

The analytical model demonstrates a clear well defined FET characteristics as shown in Figure 4.8. We can see the increase in slope of the channel current with the increase of gate to source voltage

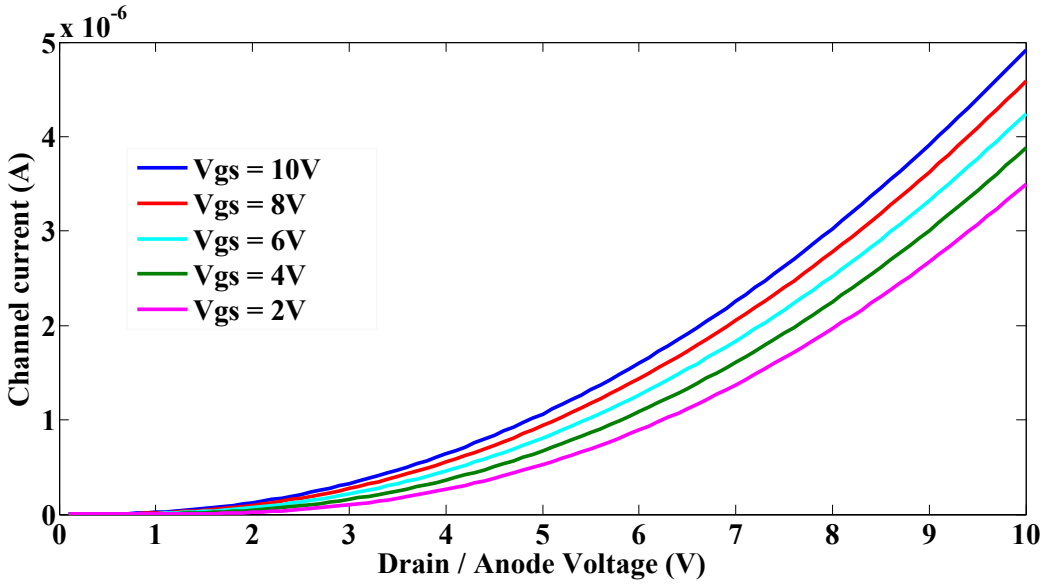

Figure 4.8 : Current-Voltage Characteristics of VFET .
For Anode to Cathode Gap of 100 nm and Tip Radius of 5 nm.

Chapter 5

Conclusion

5.1 Summary

Vacuum field emission transistor (VFET) is superior to metal-oxide-semiconductor field effect transistor (MOSFET) from a performance perspective because it uses vacuum, which is a better carrier conveyer than the semiconductors used in MOSFETs. The electrons move ballistically through vacuum with no lattice scattering. There is potential for VFET to show a higher cut-off frequency and greater power gain than the MOSFET. Furthermore, the vacuum device can be more robust than solid-state semiconductor devices under harsh operation conditions, such as high temperature and radiation environments. In unipolar semiconductor devices high temperature conditions often result in a drive current reduction and threshold voltage shift due to phonon scattering and thermionic leakage, which can degrade circuit operation. In addition, the solid-state devices are susceptible to ionizing radiations as they can cause device malfunction or even damage the circuits. There is an extra cost always paid for military, aerospace and nuclear applications through various radiation-proofing measures in order to avoid the unpredictable errors. In contrast, vacuum is inherently immune to both high temperature and radiation exposure. Nevertheless, the VFETs find only limited use in specialized applications, such as field emission displays, high-fidelity amplifiers and high power RF systems in contrast to the widespread use of MOSFET in modern electronics.

Primary hindrances to the popularity of vacuum electronics include lack of scalability, high operation voltage and short lifetime. In a step toward the implementation of full-chips comprising of VFETs, hybrid integration of VFET and other devices must be done in a synergistic manner. For example, the VFET may be assigned for the critical aspects, such as high-power and high-frequency amplifier while the MOSFET may be devoted for the non-critical parts, such as driving and register circuits. When integrating the VFET with the MOSFET, the matured technology and knowledge of MOSFET can enable a stable, uniform and predictable performance from the VFET. In this work, the nanoscale VFET is presented along with a functional MOSFET co-fabricated alongside using established CMOS technology.

Field-emission tips and arrays have made significant advances in recent years as high current density cold cathodes. Many applications of field emitter arrays are beginning to be realized, such as scanning tunneling and atomic force microscopes, and flat panel field-emission displays. The applications of FEA‘s for power tubes and accelerators are more demanding because they require many orders of magnitude higher total current and current density and typically operate at higher voltages. Areas that still require improvement for FEA‘s are integrated beam collimating lenses, higher total current, large current density modulation at gigahertz frequencies, all, of course, with long lifetime.

A number of experimental works has been done for VFET, but very few analytical works exist. A concise analytical model of this device gives the scope to explore various characteristics of the device. Proposed model includes threshold voltage, drive in voltage and channel current. It incorporates the emission physics of Child Langmuir and Fowler Nordheim. Channel current components, such as space charge limited and tunnel current have dominance in different region of device operation. Inclusion of effective electric field and emission area makes the model more accurate. The model shows good enough conformity with the available actual simulation data.

5.2 Future Course of Research Work

The cathode physics has a great deal over the performance of the vacuum field effect transistors. Sharp cathode tip is the pre-requisite for a low operating or threshold voltage. Blunt cathode tip results low emission. With the increase in the anode/drain voltage and current cathode gets hotter and thus erodes. Increase in temperature hampers current flow due to cathode resistance. In a word, it can be said that, the efficiency of the cathode thus the device is not same all along the operation range. As it has been found (Chapter 4) that, at a higher voltage proposed model shows higher deviation from the actual data. For more accuracy of the analytical model, a temperature dependent efficiency factor for cathode must be introduced and included.

There must have been a significant amount of leakage gate current with higher gate voltage. In proposed analytical model, this phenomenon has been neglected. An expression for leakage current needs to be derived. The threshold voltage been derived here shows good results for conical shaped cathodes with sharp tips. For cathode with different structures (blunt hemispherical), this model may need modification based on structural parameters.

References :

[1] Srisonphan, S.; Jung, Y. S.; Kim, H. K., –Metal-oxide-semiconductor field-effect transistor with a vacuum channel", Nature nanotechnology, 7(8), 504-508, 2012.

[2] Han, J. W.; Moon, D. I.; Oh, J. S.; Choi, Y. K.; Meyyappan, M., –Vacuum gate dielectric gate-all-around nanowire for hot carrier injection and bias temperature instability free transistor", Applied Physics Letters, 104(25), 253506, 2014.

[3] Leitenstorfer, A.; Hunsche, S.; Shah, J.; Nuss, M. C.; Knox, W. H., –Femtosecond charge transport in polar semiconductors", Physical review letters, 82(25), 5140, 1999.

[4] Kesling, W. D.; Hunt, C. E., –Beam focusing for field-emission flat-panel displays", Electron Devices, IEEE Transactions on, 42(2), 340-347, 1995.

[5] Han, J. W.; Meyyappan, M., –The device made of nothing", Spectrum, IEEE, 51(7), 30-35, 2014.

[6] Sze, S. M., –Semiconductor devices: physics and technology", John Wiley & Sons, 2008.

[7] Han, J. W.; Oh, J. S.; Meyyappan, M., –Vacuum nanoelectronics: Back to the future?—Gate insulated nanoscale vacuum channel transistor",Applied Physics Letters, 100(21), 213505, 2012.

[8] Han, J. W.; Oh, J. S.; Meyyappan, M.; –Co-fabrication of Nanoscale Vacuum Field Emission Transistor (VFET) and MOSFET", 2014.

[9] Brinkman, W. F.; Haggan, D. E.; Troutman, W. W., –A history of the invention of the transistor and where it will lead us", Solid-State Circuits, IEEE Journal of, 32(12), 1858-1865, 1997.

[10] Symons, R. S., –Tubes: Still vital after all these years", Spectrum, IEEE, 35(4), 52-63, 1998.

[11] Bardeen, J., & Brattain, W. H. (1949). Physical principles involved in transistor action. *Physical Review*, *75*(8), 1208.

[12] Noyce, R. N.; –Semiconductor Device and Lead Structures". US Patent 2,981,877 (1959).

[13] Kilby, J. S.; –Invention of Integrated Circuits". IEEE Trans. Electron Devices **ED-23**, 648 (1976).

[14] Gewartowski, J. W.; Watson, H. A.; Norstrand, D. V.; –Principles of Electron Tubes",

Co.: Princeton, NJ, p. 229, 1965.

[15] Shoulders, K. R.; Adv. Comp. **2**, 135 (1961).

[16] Moore, G. E. (1995, May). Lithography and the future of Moore's law. In *SPIE's 1995 Symposium on Microlithography* (pp. 2-17). International Society for Optics and Photonics.

[17] Langmuir, I. (1921). The structure of the helium atom. *Physical Review*, *17*(3), 339.

[18] Davisson, C. J., and L. H. Germer. "Reflection of electrons by a crystal of nickel." *Proceedings of the National Academy of Sciences of the United States of America* 14, no. 4 (1928): 317.

[19] Gehrenbeck, R. K.; "Electron diffraction: Fifty years ago", Physics Today, p. 34, January 1978.

[20] Fowler, R. H.; Nordheim, L. W.; Proc. Roy. Soc. (London), A **119**, 173 (1928).

[21] Nordheim, L. W.; Proc. Roy. Soc. (London), A **121**, 626 (1928).

[22] Binh, V.T.; Garcia, N.; Purcell, S.T.; "Electron field emission from atomic-sources: Fabrication, properties and applications of nanotips," Adv. Imaging and Electron Phys., vol. 95, pp. 63–153, 1996.

[23] Müller, E. W. (1953). *Feldemission* (pp. 290-360). Springer Berlin Heidelberg.

[24] Dyke, W. P.; Dolan, W. W.; "Advances in Electronics and Electron Physics", Vol. 8, Academic Press: New York, p. 89, 1956.

[25] Meyer, R.; Ghis, A.; Ramband, P,; Muller, F.; "Development of matrix array of cathode emitters on a glass substrate for flat display applications", in Proc. 1st IVMC, Williamsburg, VA, p. 10, 1988,

[26] Shaw, J. L.; Gray, H.F.; "Emission limiting in silicon field emitter", in Proc. 11th IVMC, Asheville, N.C., p. 146, 1998.

[27] Veen, V.; "J. Vac. Sci. Technol.", B **12**, 655 (1994).

[28] Schowebel, P. R.; Spindt, C.A.; Brodie, I.; Holland, C.E.; in Proc. 7th IVMC, Grenoble, France, p. 378, 1994.

[29] Goodhue, W.D.; Nitishin, P.M.; Harris, C.T.; Bozler, C.O.; Rathman, D.D.; Johnson, G.D.; Hollis, M.A.; "J. Vac. Sci. Technol". B **12**, 693 (1994).

[30] Dean, K. A.; Chalamala, B. R.; "Appl. Phys. Lett." **76**, 375 (2000).

[31] Zhu, W. ; Bower, C.; Zhou, O.; Kochanski, G.; Jin, S.; "Appl. Phys. Lett." **75**, 873 (1999).

[32] Komoda, T.; Sheng, X.; Koshida, N.; "J. Vac. Sci. Technol." B **17**, 1076 (1999).

[33] Driskill A.A.G.; Hasko, D.G.; Ahmed, H.; "Appl. Phys. Lett." 71, 2845–2847 (1997).

[34] Park, S.S.; Park, D.I.; Hahm, S.H.; Lee, J.H.; Choi, H.C.; Lee, J.H.; "IEEE Trans. Electron Devices" 46, 1283 (1999).

[35] Spencer, T.A.; Hendricks, J.J.; Luginsland, J.W.; Stump, M.D.; "Dynamics of the Space-Charge-Limiting Current in Gyro-Type Devices," IEEE Trans. Plasma Science **26**, 854 (1998).

[36] Stephens, K.F. ; Ordonez, C.A.; Peterkin, R.E.; "Virtual Cathode Formations in Nested-Well Configurations," in Non-Neutral Plasma Physics III, page 451, (1999).

[37] Langmuir, C.; "Discharge from Hot CaO," Phys.Rev. **32**, 492 (1911).

[38] Langmuir, C.; "The Effect of Space Charge and Residual Gases on Thermionic Currents in High Vacuum," Phys. Rev. **2**, 450 (1913).

[39] Voronin, V.S.; Zozulaya, Y.T.; Lebedev, A.N.; "Self-Consistent Stationary State of a Relativistic Electron Beam in a Drift Space," Soviet Phys. Tech. Phys. **17**, 432 (1972).

[40] Elster J.; Geitel, H.; "Becquerel rays", Wied. Ann. 66, 735 (1889).

[41] Rutherford, E.; "Radioactive substance emitted from Thorium compounds", Phil. Mag. 49, 1 (1900).

[42] Schweidler, E.R.; "Premier Congres de Radiologie", Liege (1905).

[43] Gamow, G.;"Constitution of Atomic Nuclei and Radioactivity" (Oxford University Press, London 1931).

[44] Geiger, H.; Nuttall, J.M.; "Ranges of oparticles from uranium", Phil. Mag. 23, 439 (1912).

[45] Lauhon, L.J.; Ho, W.; "Direct observation of the quantum tunneling of single hydrogen atoms with a scanning tunneling microscope", Phys. Rev. Lett. 85, 4566 (2000).

[46] Yazdani, A.; "Watching an atom tunnel", Nature, 409, 471 (2001).

[47] Jensen, K.L.; Phys. Plasmas **6**, 2241 (1999).

[48] Brodie, I.; Spindt, C.A.; "Vacuum Microelectronics" (Academic, New York, 1992).

[49] Forbes, R.G.; "J. Vac. Sci. Technol." B **17**, 526 (1999).

[50] He, J.; "Theory of Electron Emission from Atomically Sharp Metallic Emitters in High Electric Fields" (Pennsylvania State University, University Park, PA, 1992).

[51] Jensen, K.L.; Zaidman, E.G.; Kodis, M.A.; Goplen, B.A.; Smithe, D.N.; "J. Vac. Sci. Technol." B **14**, 1942,1947 (1996).

[52] Raichev, O. E.; "Coulomb blockade of field emission from nanoscaleconductors." Physical Review B 73.19 (2006): 195328.

[53] Nation, J. A., Schächter, L., Mako, F. M., Len, L. K., Peter, W., Tang, C. M., & Srinivasan-Rao, T. (1999). Advances in cold cathode physics and technology.Proceedings of the IEEE, 87(5), 865-889.

[54] Mayer, A.; "Polarization of metallic carbon nanotubes from a model that includes both net charges and dipoles". Phys. Rev. B 71, 235333 (2005).

[55] Lau, Y. Y.; Liu, Y. & Parker, R. K.; "Electron emission: from the Fowler–Nordheim relation to the Child–Langmuir law". Phys. Plasmas 1, 2082–2085 (1994).